Dispersive wave generation in supercontinuum process inside nonlinear microstructured fibre

Samudra Roy[1,3], Shyamal K. Bhadra[1,]* and Govind P. Agrawal[2]

[1]Fiber Optics and Photonics Division, Central Glass and Ceramic Research Institute (CSIR), 196 Raja S.C. Mullick Road, Kolkata 700 032, India
[2]Institute of Optics and Department of Physics and Astronomy, University of Rochester, New York, 14627, USA
[3]Present address: Graduate School of Information Science and Technology, Hokkaido University, Sapporo, Japan

The presence of higher order dispersion leads to the transfer of energy from soliton to dispersive waves (DWs: also called non-solitonic radiation), which play a significant role in blue-component generation in the supercontinuum (SC) process. The frequency of DWs is controlled by the general phase-matching condition requiring that DWs propagate with the same phase velocity as that of the soliton. In the present study, the generation of DWs in the SC process inside the nonlinear microstructured fibre/photonic crystal fibre is explored under different operational conditions. The role of third, fourth and other higher order dispersions on the generation and control of DWs is described using numerical solution of generalized nonlinear Schrödinger equation. The study reveals several important facts such as all positive, even-order dispersion terms always generate dual radiation and all odd-order dispersion produces single radiation. Even the numeric sign of the dispersion coefficient modulates the non-solitonic radiations dramatically. A more general study unfolds that dispersion profile of a specific fibre can control the generation of DWs; in fact, the zero dispersion points turn out to be excellent predictors of the number of radiation peaks being generated. It is also demonstrated that with proper tailoring of dispersion profile of nonlinear medium, it is possible to generate dual radiation in the same side of the input pulse in frequency domain. Here we have considered the case of a highly nonlinear photonic crystal optical fibre. Further, it is observed that DWs can still be generated when the pump frequency falls on the normal dispersion domain. Finally the validity of the proposed theory is established through experimental verification.

Keywords: Dispersive waves, optical solitons, photonic crystal fibres, supercontinuum generation.

SPECTRAL broadening and the generation of new frequency components are the intrinsic features of nonlinear optics. Because of these novel characteristics of nonlinear optics, it is possible to produce an artificial white light with unique spectral properties having high brightness. Under such a process an ultra short optical pulse propagating through a nonlinear medium experiences extreme spectral broadening. Owing to its broad and continuous spectrum, such extreme spectral broadening is generally called supercontinuum (SC)[1,2]. The generation of white laser in terms of SC is an important phenomenon having great physical implications. It certainly offers novel solutions in the field of optical communication, coherent tomography, multiplex light sources for nonlinear spectroscopy, biomedical lasers, etc.[3]. The mechanism of SC generation is mainly dominated by soliton dynamics when a femtosecond pulse is used as a pump, whereas four wave mixing (FWM) and nonlinear Kerr effect are considered to be the most important processes in SC generation for wider (pico or nanosecond) input pulses. In both the cases higher-order dispersions (HODs) play a significant role in modulating and controlling the spectrum. At this point it is pertinent to mention that in recent years photonic crystal fibre (PCF) has come out to be an excellent medium to support the phenomenon of SC generation owing to its high nonlinearity and flexible dispersion properties. The phenomenon of soliton dynamics is primarily involved in the SC generation process when the optical pulse is pumped in an anomalous dispersion regime. The interplay between nonlinearity and dispersion may produce stable pulse propagation in terms of optical soliton which does not change its shape in time and spectral domain during propagation[4]. The increment of input power makes the stable propagation periodic over distance. This is a feature of higher order soliton, where input pulse evolves periodically both in time and spectral domain[4]. However, under realistic condition the higher order nonlinear and dispersive effects disrupt this stable periodic evolution and split the soliton into its components through the fission process[5]. During the fission process, the presence of higher order dispersions lead to transfer of energy from soliton to narrow band resonance and associate a low amplitude temporal pedestal[6]. The radiation of dispersive waves (DWs) is also known as non-solitonic radiation (NSR) because generally its wavelength falls on the normal dispersion domain where optical soliton ceases to exist[1,2]. The frequency of the radiation emitted by the soliton in terms of DWs can readily be obtained from a phase-matching condition involving the linear and nonlinear phase change of the soliton and associated

*For correspondence. (e-mail: skbhadra@cgcri.res.in)

continuous wave[7]. The generation of DWs is physically important because of their imperative contribution in producing visible light during the SC process. The blue or UV components of the SC spectra are in fact produced through DWs. However, a suitable combination of HODs may produce radiation even in the higher wavelength side compared to input pump wavelength. An extensive study reveals that all HOD terms individually play a crucial role in generating DWs and more importantly, the growth of the radiation peaks is critically dependent on relative values of HODs and their numeric signs.

Because of the significant impact of DWs in SC generation, it requires a complete study which unfolds the physical mechanism involved in resonant radiation in the form of DWs. Though considerable amount of work has already been done in describing the phenomenon of NSR, there is ample scope to discuss elaborately the entire physical processes. Our objective here is to present a unified discussion on the various aspects of DW generation during the SC process. The present review is based on theory and extensive numerical simulations that illustrate characteristics of soliton-mediated resonant radiation covering a wide range of experimental parameters. Moreover, we perform experiments with self-made PCFs and the results are analysed with the existing theory and numerical simulation. We mainly focus on understanding the complex process of DW generation and the role of different HODs on its evolution. The present article is organized in the following fashion. First we briefly discuss about PCF and its properties. Since PCF is believed to be the most effective and dynamic nonlinear waveguide in order to produce efficient SC, it is pertinent to include a brief discussion on its nonlinear and dispersion properties. The fundamental aspects of SC generation are then described. The role of soliton dynamics in the femtosecond regime and the characteristics of experimentally generated SC are discussed by introducing the generalized nonlinear Schrödinger equation (NLSE). In the derivation we have used the convenient form of dimensionless NLSE. Finally, we elaborately study the generation of DWs in the SC process. The role of the third, fourth and all HOD terms on the evolution of DWs is explained with numerical examples. The present study would evolve certain fundamental information that may be useful for the fabrication of PCFs, which helps in controlling the generation of non-solitonic radiation. We also try to focus on the recent understanding and the new insights of the physics of soliton-mediated radiations during the SC process. The importance of the new class of optical fibre is highlighted.

Photonic crystal fibre

PCF or microstructured optical fibre (MOF) is the new generation of optical waveguides which is solely made of silica[8]. In solid-core PCFs, the central silica core is surrounded by a periodic array of air-holes running along the propagation distance. The presence of the air-holes in the cladding region eventually reduces the effective refractive index compared to the core silica and light guidance occurs through the principle of total internal reflection. The air-hole diameter (d) and their relative separation (Λ) offer additional degrees of freedom in tailoring the dispersion property[9–11]. A careful and properly designed arrangement of air-holes may produce a unique dispersion profile which is difficult to attain in conventional fibres. The dispersion in the standard telecom fibre is anomalous at wavelengths larger than 1.3 μm, whereas one can tailor the anomalous dispersion of PCF in the range 0.6–1.3 μm by suitably modulating d and Λ. Standard numerical process based on finite element method (FEM) is generally used to study the dispersion property of PCFs[12]. Owing to the tight confinement of the optical field in the small core region, PCF possesses enormous nonlinearity which is an additional advantage to excite higher order nonlinear effects. Another important aspect of PCF is its endlessly single-mode nature in which propagation of higher order modes is not observed even at short wavelengths. The reported SC generation in experiments primarily occurs through the excitation of the fundamental mode and for this reason in our numerical simulation we assume propagation only for the fundamental mode. However, in a recent study SC characteristics were also examined for multimode fibres by generalizing NLSE in femto-second regime[13]. The dispersion property of PCF is crucial in SC generation because it determines the extent to which different spectral components of an ultrashort pulse propagate at different group velocities. The identical group velocity of DWs and red-shifted soliton eventually creates a situation where blue-shifted radiation is trapped, a phenomenon experimentally observed by Nishizawa and Goto[14].

The group velocity dispersion (GVD) coefficient of an MOF is defined as follows:

$$D = -\frac{\lambda}{c}\frac{\mathrm{d}^2 n_{\mathrm{eff}}}{\mathrm{d}\lambda^2} = -\frac{2\pi c}{\lambda^2}\beta_2. \tag{1}$$

Here λ represents the wavelength, c the velocity of light and n_{eff} is defined as the effective index of the fundamental mode of MOF. The value of n_{eff} at a particular wavelength for a given MOF structure is determined numerically by FEM using commercial software, COMSOL Multiphysics. β_2 is the second-order derivative of wave number $\beta(\omega)$ over frequency (ω). In Figure 1 the photograph SEM of a highly nonlinear PCF is shown with its dispersion profile. It is found that this particular PCF structure exhibits zero dispersion ($D = 0$) around the wavelength of 987 nm.

The process of making PCF is different from conventional composite-core fibre. PCF fabrication is a two-step

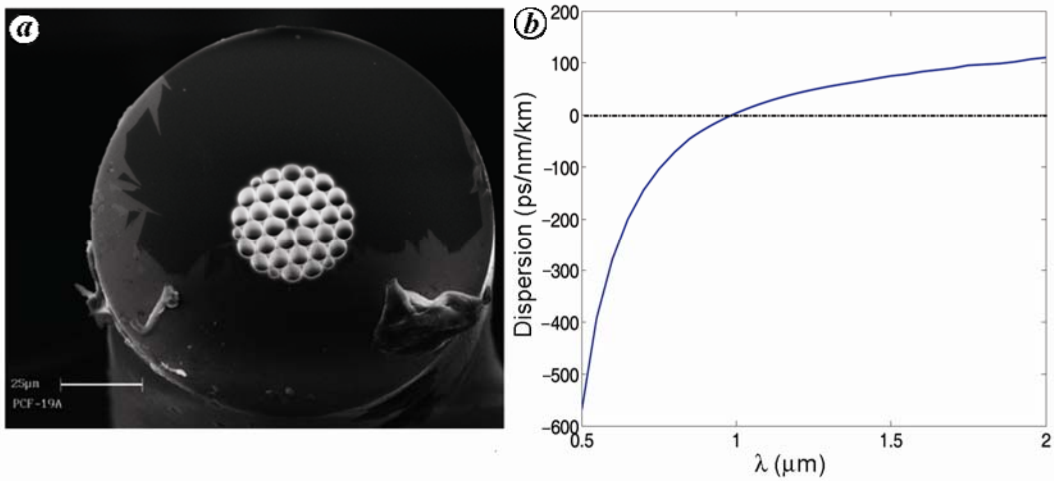

Figure 1. ***a***, SEM photograph of the cross-section of a highly nonlinear photonic crystal fibre (PCF) fabricated at the Fiber Optics and Photonics Division, Central Glass and Ceramic Research Institute (CGCRI), Kolkata. The effective area of the PCF is calculated as 8 μm^2 and air-filling fraction (d/Λ) is 0.91. ***b***, Dispersion characteristic of the same fibre. The commercial software COMSOL Multiphysics based on finite element method is used to determine the effective index (n_{eff}) of the fibre at different wavelengths. The zero dispersion wavelength of the fibre is calculated to be at 987 nm.

process. The first step consists of developing a 'preform' which contains the signature of the fibre, but on a macroscopic scale. In the second stage, the final fibre is drawn from a high-temperature furnace in a fibre-drawing tower. The main issue involving preform design and development in the case of PCFs is preservation of air-to-silica ratio in the cladding[15]. PCFs can be fabricated by several methods, including extrusion[16], sol–gel route[17], mechanical boring or milling, i.e. drilling of holes in the matrix material[18,19], etc. But a relatively simple process is the 'stack and draw' technique[20–22], which we have also adopted for fabrication of nonlinear PCFs using a precision fibre-drawing tower. This method is highly versatile, allowing complex lattices to be formed from individual stackable units or capillaries of the correct size and shape as accurate as ± 5 μm. The key parameters of PCF drawing are the furnace temperature, speed at which the preform is fed into the furnace (feed rate), fibre-drawing speed and the differential pressure within the capillaries. Precise monitoring and optimization of these parameters lead to significant modification of the geometry of the final fibre to get the desired microstructure[23,24]. It was observed that temperature of the furnace played a crucial role in the pressurization and expansion of the air-holes. Higher temperature led to increase in the air-filling fraction, whereas increase in the fibre-drawing speed lowered the fibre diameter and core diameter. After standardizing all the drawing parameters, one can achieve high air-filling fraction.

Supercontinuum generation

It has been already mentioned that SC generation is a nonlinear process where one would expect enormous spectral broadening of an ultrashort pulse during its propagation inside a nonlinear waveguide. A major part of spectral broadening is related to soliton dynamics, when an ultrashort pulse is launched in the anomalous GVD ($\beta_2 < 0$) domain[25,26]. Hence it is important to understand the basic processes involved in soliton propagation. When an optical pulse propagates inside the waveguide, the dispersion and nonlinear property both introduce additional phase. Physically, the phase induced by the dispersion depends on its numeric sign and in anomalous dispersion domain (i.e. for negative sign of dispersion) it counter balances the additional phase introduced through nonlinear self-phase modulation (SPM)[4]. Because of this cancellation process, pulse broadening ceases to occur and one would expect optical soliton. The most standard equation that mathematically describes the propagation of an optical soliton is given as[4]

$$i\frac{\partial U}{\partial \xi}+\frac{1}{2}\frac{\partial^2 U}{\partial \tau^2}+N^2|U|^2U=0. \tag{2}$$

The general solution can readily be obtained as $U(\xi, \tau) = N\text{sech}(\tau)\exp(\text{i}\xi/2)$, where $N = 1$ characterizes fundamental soliton and $N > 1$ for higher order solitons (HOS).

The order of soliton N is defined as $(L_{\text{D}}/L_{\text{NL}})^{1/2}$, where $L_{\text{D}} = T_0^2/|\beta_2|$ is the dispersion length and $L_{\text{NL}} = 1/\gamma P_0$ is the nonlinear length with T_0, P_0 and γ being the pulse width, peak power and nonlinear coefficient respectively. For $N > 1$, the optical soliton evolves periodically both in temporal and spectral domain. The stable periodic evolution of HOS disrupts significantly because of the presence of HOD and higher order nonlinearity, viz. Raman scattering, self-steepening, etc. The perturbing effects result in pulse break-up through the soliton fission process, where a HOS splits into its components and

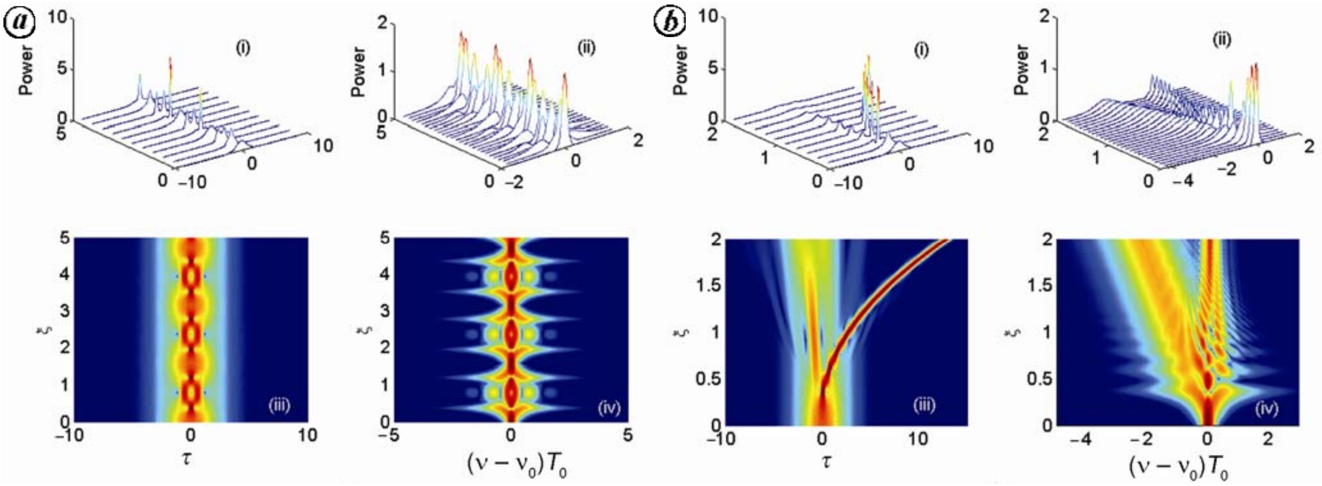

Figure 2. ***a***, Temporal and spatial evolution of a third-order soliton ($N = 3$) in an ideal condition without any perturbation. ***b***, Evolution of the same soliton perturbed under the intra-pulse Raman Scattering (IPRS) process. The fission takes place roughly around $1/N$ normalized distance which comes out to be 0.33 for $N = 3$ and is evident from plot (iii). The frequency downshifting characterized by IPRS is clearly observed in plot (iv), where it is shown how a major part of pulse energy is shifted to the lower frequency side.

ejects from the input pulse in an ordered fashion, one by one. The highest peak power soliton, generally called Raman soliton exhibiting largest group velocity difference from pump, is delayed most in time domain during propagation. A theoretical treatment reveals that the Nth order soliton splits into its components having amplitude $A_k = A_0(2N - 2k + 1)/N$ and width $T_k = T_0(2N - 2k + 1)^{-1}$, where k takes the value from 1 to N representing the individual components[5]. The separation of the individual components of the soliton is physically controlled by the momentum conservation principle. An ideal propagation of an optical soliton of order three is captured in Figure 2 *a*. The periodic temporal and spectral evolutions are shown in plots (i) and (ii). In Figure 2 *b*, the fission process is shown where a third-order soliton is perturbed by intra-pulse Raman scattering (IPRS)[4]. Plot (iii) readily shows how Raman soliton is delayed and plot (iv) captures the Raman frequency downshifting.

To capture different nonlinear effects in the process of SC generation, it is essential to solve the generalized NLSE numerically. The normalized form of the generalized NLSE in the anomalous dispersion domain ($\beta_2 < 0$) can be obtained as

$$\frac{\partial U}{\partial \xi} = \frac{i}{2}\frac{\partial^2 U}{\partial \tau^2} + \sum_{m\geq 3}^{\infty} i^{m+1}\delta_m \frac{\partial^m U}{\partial \tau^m} + iN^2\left(1 + is\frac{\partial}{\partial \tau}\right)$$
$$\times\left(U(\xi,\tau)\int_{-\infty}^{\tau} R(\tau-\tau')\left|U(\xi,\tau')\right|^2 \mathrm{d}\tau'\right), \qquad (3)$$

where the field amplitude $U(\xi, \tau)$ is normalized such that $U(0, 0) = 1$ and the other dimensionless variables are defined as:

$$\xi = \frac{z}{L_D}, \quad \tau = \frac{t - z/v_g}{T_0}, \quad N = \sqrt{\gamma P_0 L_D} \text{ and}$$

$$\delta_m = \frac{\beta_m}{m!\,T_0^{m-2}\,|\beta_2|}. \qquad (4)$$

Here P_0 is related to the peak power of the ultrashort pulse launched into the fibre, T_0 is the input pulse width, v_g the group velocity, γ the nonlinear parameter of the fibre, $s = (2\pi v_s T_0)^{-1}$ is the self-steepening parameter and $R(\tau)$ the nonlinear response function of the optical fibre in the form

$$R(\tau) = (1 - f_R)\delta(\tau) + f_R h_R(\tau), \qquad (5)$$

where $f_R = 0.245$ and the first and the second terms correspond to the electronic and Raman responses respectively. As discussed by Lin and Agrawal[27], the Raman response function can be expressed in the form

$$h_R(\tau) = (f_a + f_c)h_a(\tau) + f_b h_b(\tau), \qquad (6)$$

where the functions $h_a(\tau)$ and $h_b(\tau)$ are defined as

$$h_a(\tau) = \frac{\tau_1^2 + \tau_2^2}{\tau_1 \tau_2^2}\exp\left(-\frac{\tau}{\tau_2}\right)\sin\left(\frac{\tau}{\tau_1}\right),$$

$$h_b(\tau) = \left(\frac{2\tau_b - \tau}{\tau_b^2}\right)\exp\left(-\frac{\tau}{\tau_b}\right), \qquad (7)$$

and the coefficients $f_a = 0.75$, $f_b = 0.21$, and $f_c = 0.04$ quantify the relative contributions of the isotropic and

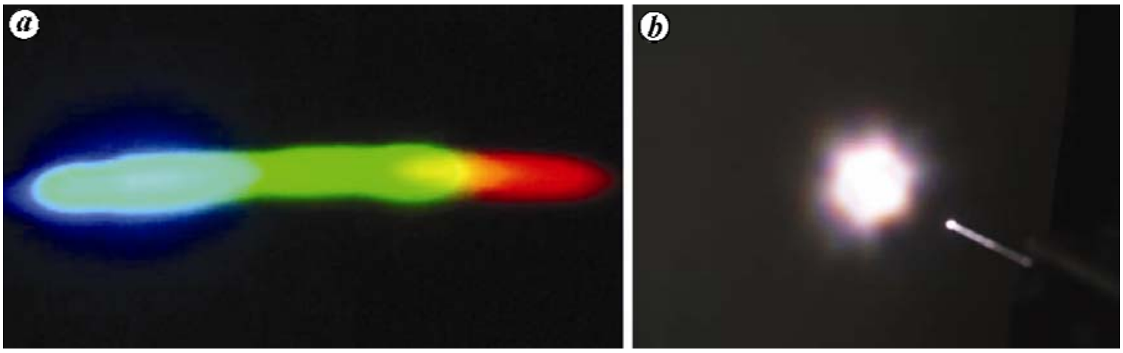

Figure 3. ***a***, Visible part of the supercontinuum (SC) spectra under femtosecond pumping. The fibre used is same as that shown in Figure 1 *a*. ***b***, White-light generation through SC process. The experiment was done at the Fiber Optics and Photonics Division, CGCRI, Kolkata.

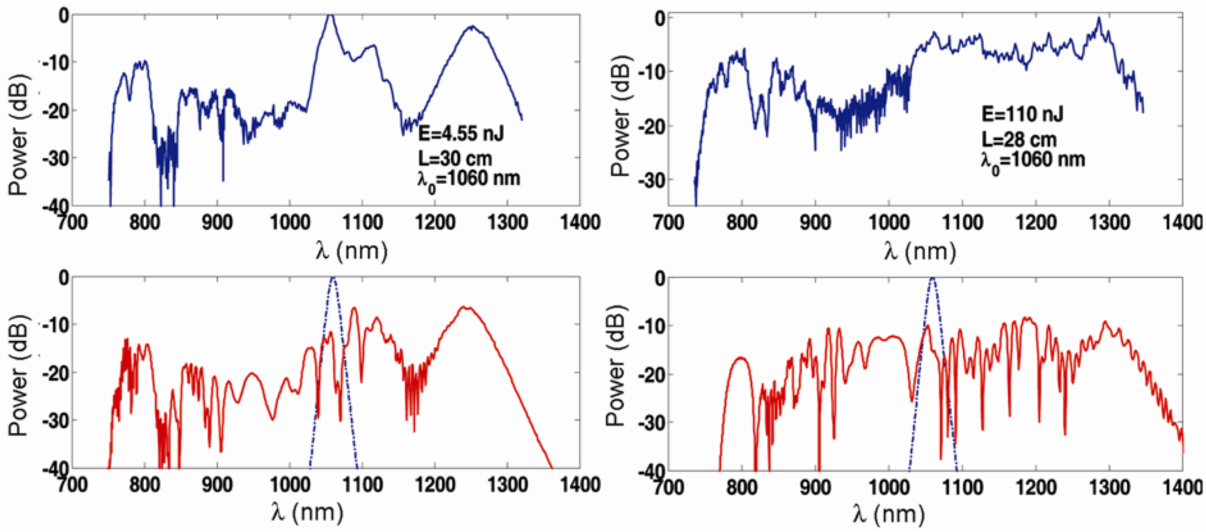

Figure 4. Experimental and the corresponding numerical simulation of SC generation in two different highly nonlinear PCFs. The blue curve represents the experimental spectra, whereas the numerical solutions are given by red curves. The input pulse width was 110 fs in both cases.

anisotropic parts of the Raman response. In eq. (7), τ_1, τ_2 and τ_b have values of 12, 32 and 96 fs respectively. In our notation, they have been normalized by the input pulse width T_0.

The numerical solution of eq. (3) using split-step method[4] proves to be an excellent tool in understanding the intermediate processes of SC generation. The experiment for generating ultra-broadband spectra in femtosecond regime is performed using the highly nonlinear PCF as shown in Figure 1, and the visible part of the generated SC spectra is depicted in Figure 3.

The experimental SC spectra are comprehensively modelled by the numerical solution of the generalized NLSE as shown in Figure 4. The figure depicts SC generation for two different PCFs designed and fabricated at the Central Glass and Ceramic Research Institute (CGCRI), Kolkata. The corresponding simulated results (red curves) based on the numerical solution of generalized NLSE predict the experimental spectra quite reasonably. The simulations give an idea about the evolution pattern of SC during propagation. In both the cases we find distinct blue peaks around 800 nm wavelength, which are generated because of the radiation of DWs.

The process of SC generation mainly comprises three distinct processes. (i) Initial symmetric spectral broadening due to SPM; (ii) Generation of red component because of Raman frequency downshifting, and (iii) DW generation which creates the visible part of the spectra. To explore these entire processes conveniently, we adopt another interesting technique called the frequency resolved optical gating (FROG) or spectrogram. The technique provides simultaneous information about pulse shape and spectrum at a particular distance. Mathematically, the spectrogram is described as

$$S(\tau,\omega)=\left|\int_{-\infty}^{\infty} U(L,t)W(L,t-\tau)\exp(\mathrm{i}\omega t)\mathrm{d}t\right|^2, \tag{8}$$

where U is the output pulse, W the reference window function generally taken as Gaussian, L the fibre length and τ is an adjustable delay. The spectrogram as shown in Figure 5 interprets different SC features that would be of importance in understanding the process. The plot immediately identifies DWs, Raman soliton component and their correlation. The parabolic group delay variation over wavelength indicates that Raman soliton and DWs propagate with identical group velocity and the blue radiation is hence trapped, as observed experimentally[14]. We have separately calculated the delay using HOD coefficients and it is represented as a white dotted line in Figure 5. The intensity of the Raman soliton is stronger than DWs. So the cross phase modulation (XPM) induced by the Raman soliton on DWs is significant. The interaction of Raman soliton and DWs in fact generates new frequencies under the XPM process. This feature can only be observed in the spectrogram representation and in Figure 5 it is indicated by a red circle.

Dispersive waves: a theoretical development

The perturbation theory of soliton propagation was studied extensively in the early 90s by several groups[28–31]. Enquiring the effect of dispersion, all the results predicted the side band in spectral domain. A more elaborate study by Akhmediev and Karlsson[7] finally revealed the phase-matching condition associated with NSR and theoretically predicted the radiation amplitudes. The blue-shifted NSR in the formation of SC was further elaborated by Husakou and Herrmann[32]. In the same year a detailed experiment was conducted to understand the solitonic phenomena such as pulse-breaking and low-amplitude radiation in generating ultra-broad SC spectra[33]. In a more comprehensive study by Dudley *et al.*[34], the temporal and special characteristics were further resolved using cross-correlation frequency resolved optical gating (XFROG) trace. The physical origin of DWs and their evolution was demonstrated well[34]. The strong blue radiation in the form of DWs was again experimentally studied[35] and a tentative proposal was made in explaining the generation of DWs by invoking pulse-trapping phenomenon, which is controlled by the group velocity matching among infrared and visible pulses. The formation and behaviour of a blue-shifted, non-solitonic component, emitted as the soliton evolves towards the stable regime, was studied and the role of phase matching through higher-order dispersion was highlighted by Hilligsøe *et al.*[36]. The mechanism of the visible peak being generated in SC spectra was explained in a study[37] which revealed that the process of DW generation is initiated when a higher order optical soliton contracts in a manner that the corresponding spectrum overlaps the resonant DW region. It was further shown that DW may generate for each incidence when extended soliton spectrum overlaps the UV region in frequency domain during propagation. The investigation of XPM between the soliton and DW was examined by Genty *et al.*[38] for sub femtosecond pulses. It was shown that XPM plays a significant role in extending the SC band towards lower wavelength. The interaction of optical soliton with DW was further studied by Eflimov *et al.*[39], who demonstrated that interaction of the orthogonally polarized DW and soliton results in the generation of new resonant frequencies under the condition when four-wave mixing is not phase matched. The role of two zero dispersion profiles and their effect on DW generation was another interesting aspect studied extensively[40,41]. Practically, the enhancement of fourth-order dispersion (4OD) is directly related to the occurrence of two zero dispersion points in the dispersion profile. In a later section we elaborately discuss the specific condition where 4OD primarily affects the generation of NSR.

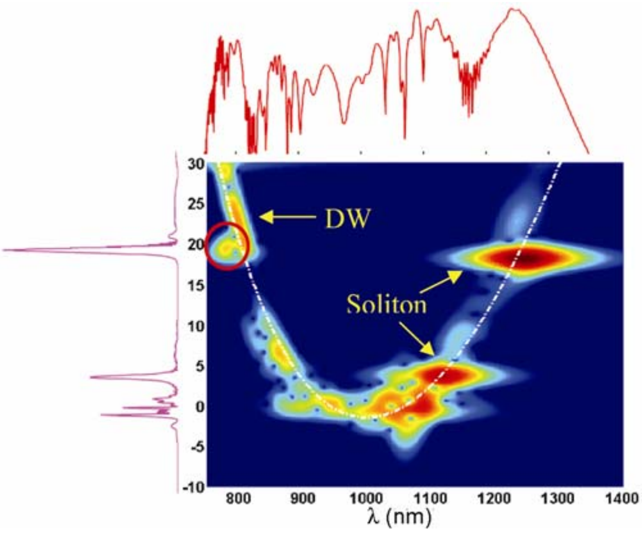

Figure 5. Spectrogram at propagation distance of 30 cm. It correlates the spectral and temporal evolution during the SC process. In the x-axis wavelength is plotted, whereas the normalized relative group delay is plotted along y-axis. The delay curve, calculated from the given dispersion values, is superimposed as a white doted line. The cross phase modulation (XPM) induced frequency component is indicated by red circle.

The soliton fission process alone does not produce high-frequency spectral component in normal dispersion regime. Generation of DWs plays a pivotal role in expanding the wide spectrum in extreme blue or UV region, which generally falls in the normal dispersion domain for a PCF. The low-amplitude temporal background pulses which are generated after the fission process and clearly observed in all numerical simulations, cannot be explained through only the soliton fission phenomenon. In order to obtain satisfactory answers for these questions, it is necessary to study the role of higher order dispersion on soliton fission process. The presence of HOD terms modifies the soliton fission process in two distinct ways. First, the ejected fundamental soliton in the fission process experiences varying second-order dispersion (2OD) at different

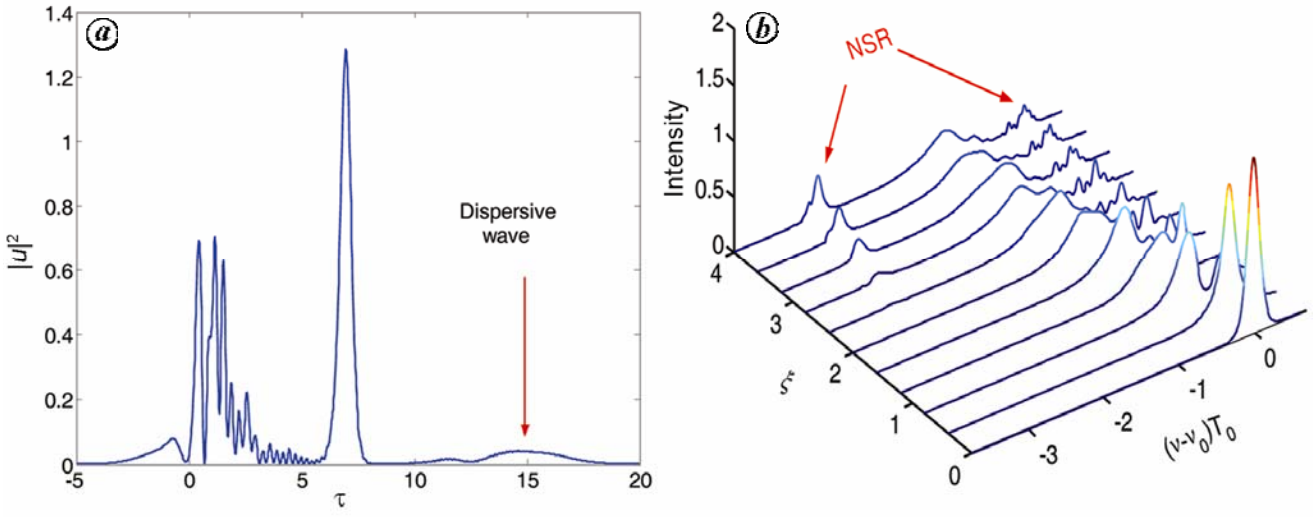

Figure 6. ***a***, Low-amplitude pedestal in the form of dispersive wave (DW). ***b***, Non-solitonic radiation (NSR) in spectral domain under two zero dispersion conditions where fourth-order dispersion (4OD) is dominant.

points. Accordingly, it adjusts its peak power and temporal width to conserve the soliton energy. Secondly, the presence of HOD leads to the transfer of energy from the soliton to a narrow band resonance radiation in the normal dispersion regime and accordingly, develops a low-amplitude temporal pedestal. In Figure 6, generation of DWs in time domain as well as frequency domain is shown. It should be mentioned that, it is not necessary to generate DWs in only normal dispersion regime; in certain conditions and for specific dispersion profiles, DWs may be generated in anomalous dispersion domain.

Normally a DW cannot be phase-matched with a fundamental soliton whose wavenumber lies in a range forbidden for a linear DWs. However, the presence of HODs can lead to a phase-matched situation in which energy is transferred from the soliton to DW at a specific frequency[4,6,7]. The frequency of NSR is governed by a simple phase-matching condition which can be given as

$$\sum_{m=2}^{\infty} \frac{\beta_m(\omega_s)}{m!}(\omega_d - \omega_s)^m = \frac{1}{2}\gamma P_s, \qquad (9)$$

where ω_s and ω_d are the frequencies of the soliton and DW respectively. The different orders of dispersion are indicated by the integer m. P_s is peak power of the Raman soliton formed after fission process and γ is the nonlinear coefficient. The RHS of eq. (9) is introduced because of the additional nonlinear phase experienced by the soliton. The phase-matching condition clearly indicates that the frequency of DW critically depends on the operating wavelength. It also suggests that if we do not include higher order terms ($m > 2$) in the equation, then we cannot get any real solution for a DW to occur when the soliton propagates in the anomalous dispersion ($\beta_2 < 0$) region. Hence theoretically the presence of third-order dispersion (3OD) is the primary condition to generate DWs when the optical pulse propagates as a soliton. In fact, in Figure 7 we demonstrate how 3OD leads to NSR. As shown in Figure 7 *a*, in the absence of 3OD there is absolutely nothing in the lower wavelength range, but the situation changes dramatically with the introduction of 3OD. A distinct radiation peak generated through DW is observed around 675 nm for nonzero 3OD coefficient as shown Figure 7 *b*. Another important observation is that the frequency of the red-shifted pulse due to the IPRS process significantly reduces because of the generation of DWs at the low frequency side. Fundamentally, the momentum conservation principle is responsible for the reduction of frequency in red shifting.

It is obvious that the radiation wavelength/frequency and peak amplitude of DW depend on the numeric value of the 3OD coefficient. In the next section we will discuss in detail the influence of 3OD coefficient on the evolution of DW or NSR.

Role of 3OD in generation of DW

Akhmediev and Karlsson[7] proposed an analytical expression for the frequency and amplitude peak of NSR generated in the output spectrum because of the perturbation of 3OD. In the present study we have generalized the work of Akhmediev and Karlsson by introducing HOS and all higher order nonlinear effects. It turns out that the perturbation of 3OD manifests through emission of NSR at a different frequency that is associated with the soliton[28]. DW normally cannot be phase-matched with the soliton whose wavenumber lies in a range forbidden for a linear DW. However, the presence of 3OD can lead to a phase-matched situation in which energy is transferred from the soliton to DW at a specific frequency. Considering up

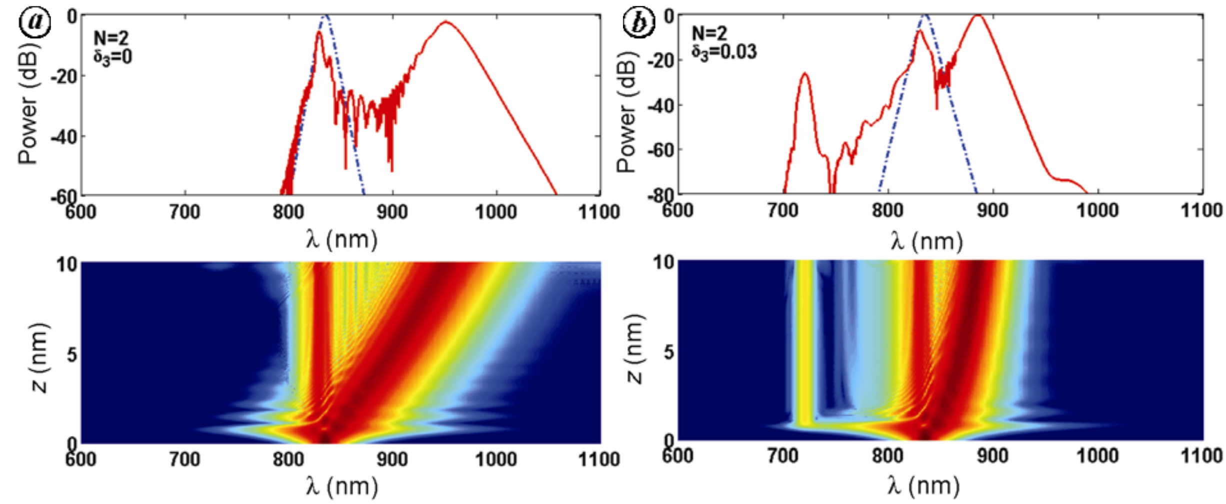

Figure 7. ***a***, Spectrum of a second-order soliton ($N = 2$) in the absence of third-order dispersion (3OD) at 10 m of propagation distance. ***b***, Spectrum of a second-order soliton in the presence of 3OD, where DW is generated distinctly around the wavelength of 675 nm.

to $m = 3$, the phase matching condition as given in eq. (9) can simply be written as

$$\Omega_d \approx -\frac{3\beta_2}{\beta_3} + \frac{\gamma P_0 \beta_3}{3\beta_2^2}, \qquad (10)$$

where $\Omega_d = \omega_d - \omega_s$, the frequency difference between the DW (ω_d) and the soliton (ω_s). Here only 3OD is considered. Based on the given phase-matching condition, one can predict the radiation frequency. In our notation, this frequency is given by a relatively simple dimensionless expression[7]

$$\Delta\nu_d T_0 \approx \frac{(1+4\delta_3^2)}{4\pi\delta_3}, \qquad (11)$$

where $\Delta\nu_d = \nu_d - \nu_s$, and ν_s and ν_d are the carrier frequencies associated with the soliton and DW respectively. δ_3 is the normalized 3OD coefficient as defined in eq. (4). It is also possible to calculate the peak power level P_d of the NSR, and the relative power (p_d), correct to first-order in δ_3, is given by[7]

$$p_d = \frac{P_d}{P_0} \approx \left(\frac{5\pi}{4\delta_3}\right)^2 \left[1 - \frac{2\pi}{5}\delta_3\right]^2 \exp\left[-\frac{\pi}{2\delta_3}\right]. \qquad (12)$$

One may ask whether eqs (11) and (12) apply when the input pulse propagates as a higher-order soliton ($N > 1$), the situation encountered commonly for SC generation. In this case, 3OD and IPRS induce the fission of the higher-order soliton, such that the Nth-order soliton splits into N fundamental solitons of different widths and amplitudes. As mentioned earlier, the most energetic soliton (Raman soliton) has a width T_s that is $(2N - 1)$ times smaller than the input pulse width T_0 and its peak power is larger by a factor of $(2N - 1)^2/N^2$ (ref. 5). The theory in Akhmediev and Karlsson[7] should be applied to this soliton because it is perturbed the most by 3OD. The frequency and the amplitude of DW can again be obtained using the same procedure, and the result is found to be[42]

$$\Delta\nu_d T_0 \approx \frac{1}{4\pi\delta_3}[1 + 4\delta_3^2(2N-1)^2], \qquad (13)$$

$$p_d \approx \left(\frac{5\pi N}{4\delta_3}\right)^2 \left[1 - \frac{2\pi}{5}(2N-1)\delta_3\right]^2 \exp\left[-\frac{\pi}{2(2N-1)\delta_3}\right]. \qquad (14)$$

It should be stressed that eqs (13) and (14) apply only for the shortest soliton (with maximum peak power), which is primarily responsible for generating NSR. Other solitons also produce DWs, but their amplitudes remain relatively low. Figure 8 *a* and *b* shows how the NSR power p_d varies with δ_3 for a fixed N, and with N for a fixed δ_3, respectively, using the analytical result given in eq. (14). In both cases, we assume that a relative power level of 10^{-8} (or –80 dB) is the lowest limit for the formation of the NSR peak in the output spectrum. We note that a minimum value of δ_3 is needed before the onset of NSR, but this value depends strongly on the soliton order N. For example, δ_3 should exceed 0.06 for $N = 1$, but this value is reduced to below 0.02 for $N = 2$. Once the NSR peak is formed, its amplitude grows rather rapidly with both δ_3 and N because of the exponential term in eq. (14). We should also stress that the validity of eq. (14) becomes doubtful once the relative power of NSR has reached a level close to −15 dB, because of a perturbative approach requiring $(2N - 1)\delta_3 \ll 1$ used to derive it.

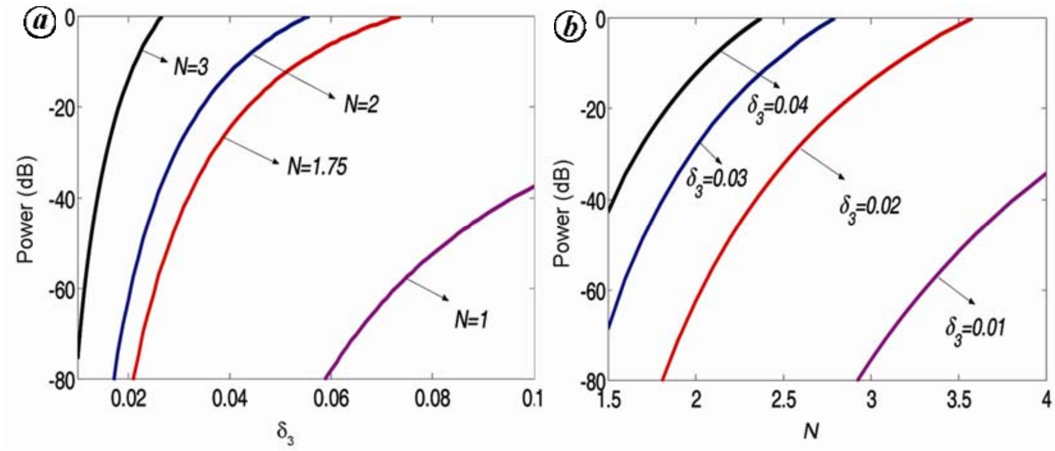

Figure 8. Variation of NSR power (***a***) with the 3OD parameter δ_3 and (***b***) with the soliton order N based on the analytic result in eq. (14).

We note from Figure 8 that the normalized 3OD parameter δ_3 plays a crucial role in controlling NSR generation. Even a small change in the value of δ_3 can make a relatively big difference in the peak power level of the NSR. Being dimensionless, one can get the same value of δ_3 for many different combinations of β_2, β_3 and T_0. With this feature in mind, in this section we study numerically how the amplitude and the frequency of the NSR peak vary with δ_3 for a given soliton order N. In particular, we focus on the $N = 2$ case.

An interesting question is how much the NSR amplitude and frequency are affected by the IPRS-induced red shift of the shortest soliton created through the fission process. Figure 9 *a* shows the frequency, and Figure 9 *b* the relative power of the NSR peak as a function of δ_3 for the second-order soliton ($N = 2$) with (circles) and without (stars) the higher-order nonlinear effects. Although the frequency of the NSR peak is not much affected by IPRS, the amplitude of this peak is reduced significantly because of IPRS, especially for low values of δ_3 for which this reduction may exceed a factor of 20 dB. The continuous transfer of energy initiated by IPRS towards longer wavelengths may be responsible for this feature. Note that the amplitude of the DW first increases rapidly with increasing δ_3 (up to $\delta_3 = 0.04$ approximately), but then saturates for values of $\delta_3 > 0.05$. Note also that it becomes difficult to separate the NSR peak from the rest of the pulse spectrum when δ_3 exceeds 0.1, because of the inverse dependence of $\Delta\nu_d$ on δ_3.

The dot–dashed lines in Figure 9 show the analytical prediction based on eqs (13) and (14). The numerical results for the NSR frequency in Figure 9 *a* agree well with this prediction for low values of δ_3. The agreement is reasonable even for higher values of δ_3, even though the numerical values are consistently larger by about 5% or so. What is surprising is that the NSR frequency does not change much when IPRS is included. One possible explanation is that the NSR peak is generated right after the soliton fission. At that point, IPRS has not yet produced any spectral changes, and the prediction of eq. (13) applies. Even though IPRS continuously shifts the soliton frequency toward the red side beyond this point, and the value of δ_3 changes because of changes in β_2 and β_3, it appears that these changes have no impact on the NSR frequency. The situation is quite different as far as the amplitude of the NSR peak is concerned. The dot-dashed line in Figure 9 *b* falls quite close to the numerical results obtained with the full NLSE that includes the higher-order nonlinear effects, but it deviates considerably from the data obtained in the absence of IPRS. In deriving eq. (14), we used the peak power and pulse width of the shortest soliton, generated by the fission process and shifting the most towards the red side because of IPRS. The results show that our approximate analytical results given in eqs (13) and (14) can be used to predict the frequency and amplitude of the NSR peak under realistic conditions, as long as δ_3 is not too large, because the analytic results are valid only for relatively small values of δ_3 due to their perturbative nature. This is especially true in the case of the NSR amplitude. As seen in Figure 9 *b*, the relative power of the NSR peak saturates to a value close to 10% of the input peak power. This is what one would expect on physical grounds. Hence the study reveals that with increasing value of 3OD coefficient, the resonant frequency becomes closer to the frequency of the input soliton with increasing peak amplitude. A relevant question at this point is what would happen if we make 3OD negative. For negative 3OD coefficient ($\delta_3 < 0$), the radiation falls in the lower frequency side.

Role of 4OD in generation of DW

Fourth-order dispersion is the next significant term after 3OD that influences NSR resulting in the generation of dual radiation[43]. The existing theory[7] suggests that the

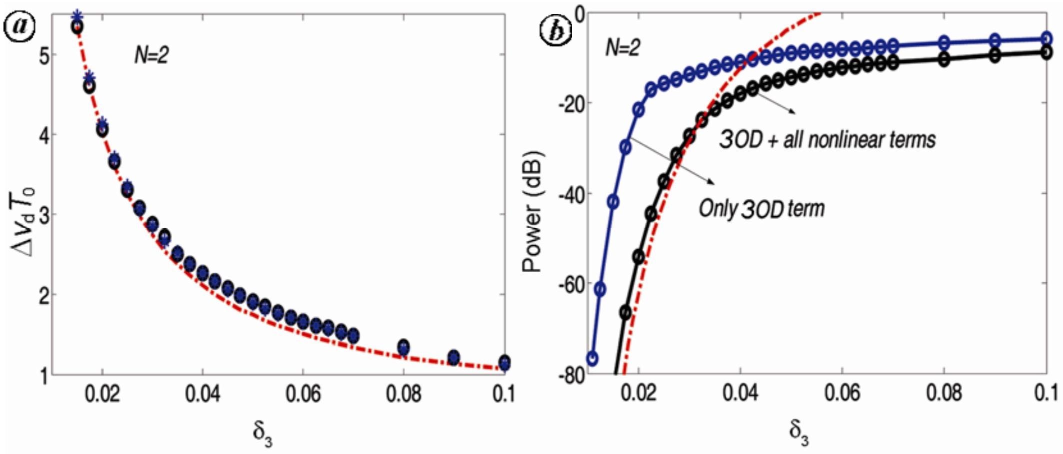

Figure 9. Frequency shift (***a***) and relative peak power of the NSR peak (***b***) plotted as a function δ_3 (circles) and estimated from the numerically calculated output spectra. Dot–dashed lines show the analytical prediction based on theory as given in eqs (13) and (14). Star symbol shows the results obtained when higher-order nonlinear effects are neglected.

positive 4OD always generates a conjugate radiation where a blue and red peak are observed in the output spectrum. The extensive numerical simulation confirms the fact that in the absence of higher order nonlinear effect and other dispersion terms, the dual peaks generated through 4OD are placed symmetrically in the frequency domain. At this point it is pertinent to mention that in the following sections the high frequency and low frequency NSR will frequently be represented as 'blue radiation' and 'red radiation' respectively. The terms 'blue' and 'red' are loosely used only to indicate the high and low frequency radiations with respect to input frequency. Hence it is suggested not to confuse the 'blue' and 'red' terms by considering them as actual blue and red radiations.

In the SC generation process, HOD and IPRS act as perturbations that split the Nth-order soliton into N fundamental solitons of different widths and amplitudes. The shortest and most energetic soliton has a width T_s that is $(2N-1)$ times smaller than the input pulse width T_0 and its peak power is larger by a factor of $(2N-1)^2/N^2$ (ref. 5). Hence the phase-matching expression given in eq. (9) can be represented in the following normalized form

$$\sum_{m=2}^{\infty} \delta_m x^m = \frac{1}{2}(2N-1)^2, \tag{15}$$

where N stands for soliton order, $x = 2\pi(\nu_d - \nu_s)T_0$, and ν_s and ν_d are the carrier frequencies associated with the soliton and DW, respectively.

Expanding eq. (15) up to fourth order ($m = 4$), one may have a polynomial whose real solutions identify the frequencies of the possible NSRs. In the present case we consider a condition where 3OD vanishes and only the 4OD term is present. This situation gives two symmetric solutions and in the simulation we get almost two symmetric frequency positions around ± 1.75 indicating NSR, as shown in Figure 10 *b*. The phase-matching expression also identifies the exact frequency of the radiations. The overall asymmetry in the spectrum arises due to the presence of higher-order nonlinear terms.

Figure 10 shows several interesting facts regarding the dual radiation generated by 4OD. The generation of low-amplitude pedestals in time domain is an important feature that is observed during DW generation. This effect is shown in Figure 10 *a*, where in an extended scale (middle plot) one can clearly identify the pedestal waves. More interestingly, these radiations travel at different speeds inside the fibre. Red radiation travels faster whereas blue radiation travels slower than the Raman soliton.

In order to study the individual effect of 4OD it is essential to use the simple model of NLSE which is given as follows

$$i\frac{\partial U}{\partial \xi} + \frac{1}{2}\frac{\partial^2 U}{\partial \tau^2} + N^2|U|^2U$$

$$= i\delta_3\frac{\partial^3 U}{\partial \tau^3} - \delta_4\frac{\partial^4 U}{\partial \tau^4} + i\tau_R\frac{\partial |U|^2}{\partial \tau}, \tag{16}$$

where $\tau_R = T_R/T_0$ and T_R is the IPRS coefficient with a value of about 3 fs. This model assumes that the pulse bandwidth is a small fraction of the Raman shift (about 13.2 THz for silica fibres) and is thus valid for pulses longer than 1 ps.

We used a standard split-step Fourier method[4] to solve eq. (16) numerically. Figure 11 shows the output spectra and the corresponding spectrogram at propagation distance of four dispersion lengths and for soliton order of 2. Figure 11 plot (i) shows the idealized situation in which only the 4OD term acts as a perturbation ($\delta_4 = 0.001$), i.e. we set $\delta_3 = 0$ and $\tau_R = 0$. As expected from the

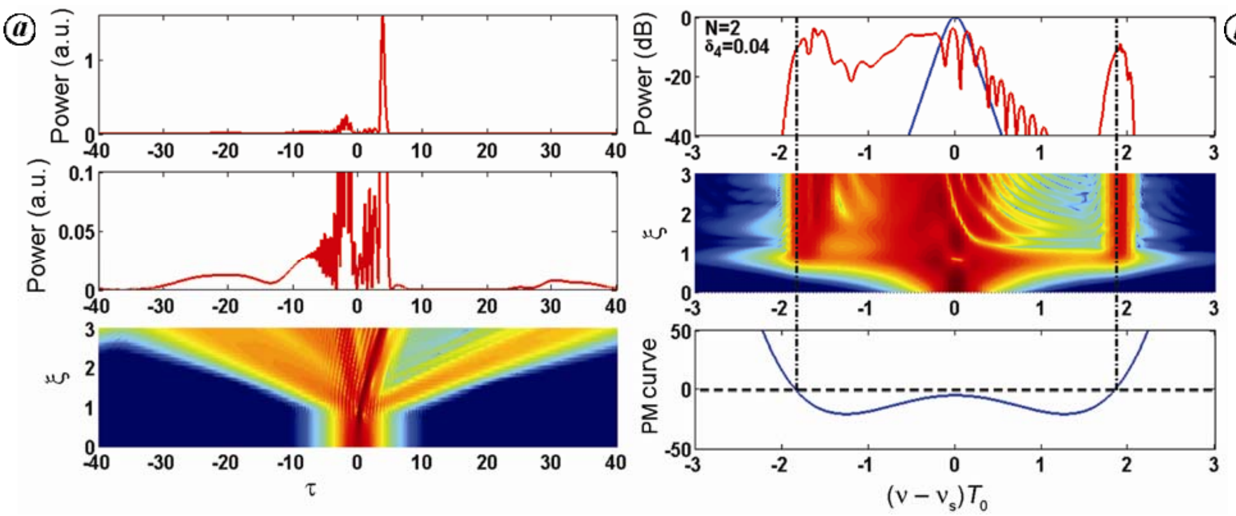

Figure 10. Effect of 4OD in temporal and frequency domain. ***a***, Generation of two DWs is shown for a second-order soliton ($N = 2$). The low amplitude pedestals are represented in extended scale. ***b***, The corresponding spectrum is shown where the phase matching curve identifies the two radiation peaks generated in the blue and red side of the input frequency.

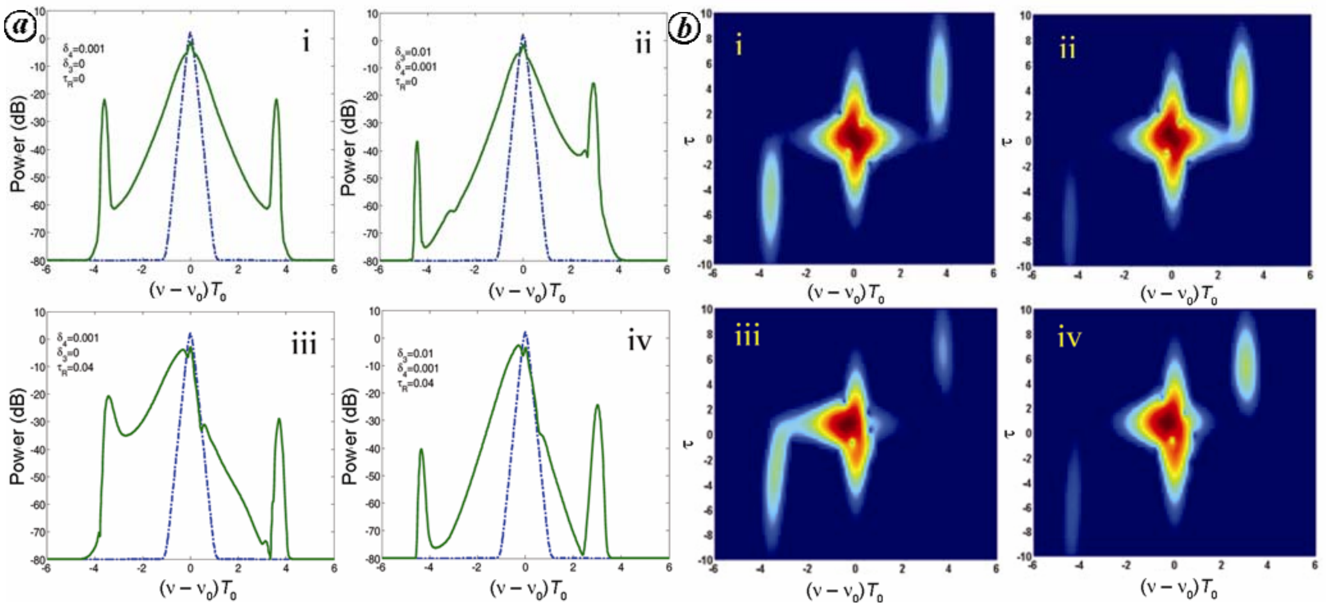

Figure 11. ***a***, Output spectra after four dispersion lengths for four different combinations of δ_3, δ_4 and τ_R. Input pulse excites a second-order soliton ($N = 2$) that splits into two fundamental solitons soon after the pulse having initial frequency ν_0 is launched inside an optical fibre. ***b***, Spectrograms of the corresponding spectra.

theory[7], 4OD creates two spectral peaks located symmetrically on the red and blue side of the input carrier frequency. Figure 11 plot (ii) shows how these NSR peaks are affected by the presence of 3OD ($\delta_3 = 0.01$). As one would expect, the presence of 3OD destroys the symmetric nature of the NSR peaks. At the same time, the amplitude of the blue peak increases whereas that of the red peak decreases. The frequency changes induced by a finite value of the 3OD parameter are expected from the phase-matching condition given in eq. (15). It should be noted that, being dimensionless quantities, one can get the same values of δ_3, δ_4 and N for many different combinations of the pulse parameters T_0 and P_0, and fibre parameters β_2, β_3 and β_4. Our results indicate that the resulting output spectrum will be the same in all cases as long as the dimensionless parameters δ_3, δ_4 and N have the same values. We study next how the amplitudes and the frequencies of the two NSR peaks are affected by the IPRS, a process that transfers part of the pulse energy towards longer wavelengths. Figure 11 plot (iii) shows the influence of IPRS on the output pulse spectrum in the presence of 4OD alone ($\delta_3 = 0$). As one may expect, the spectrum becomes asymmetric because of a continuous transfer of energy from high frequencies to low

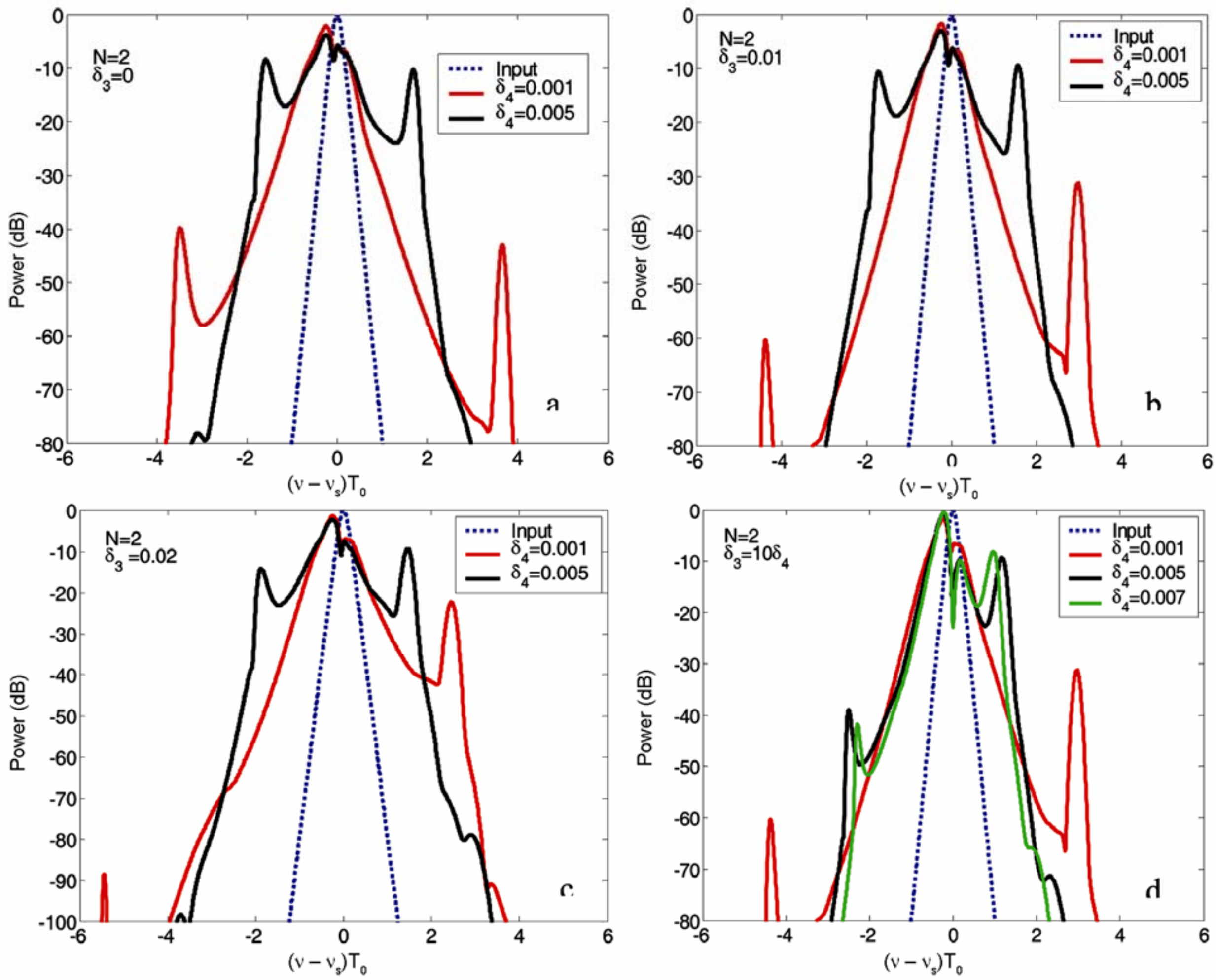

Figure 12. Output spectra after one dispersion length for different combinations of δ_3 and δ_4. The generalized NLSE given in eq. (3) is solved numerically for a femtosecond input pulse with T_0 = 50 fs. The soliton frequency is given by ν_s.

frequencies[3]. However, notice that neither the positions nor the amplitudes of the NSR peaks are affected much by the IPRS process. This feature indicates that DWs are generated right after the soliton-fission process and their frequencies and amplitudes are not affected by the subsequent energy transfer induced by IPRS. In Figure 11 plot (iv) we include the effects of 3OD and IPRS simultaneously and obtain the output spectrum under a more general and realistic situation. The spectrum is changed significantly from that seen in Figure 11 plot (iii). In particular, we find that the blue side of the pulse spectrum contains more pulse energy compared to the red side. This is related to the fact that 3OD by itself creates an NSR peak on the blue side of the spectrum when $\delta_3 > 0$. Even though a single peak occurs on the blue side in the presence of both 3OD and 4OD, its amplitude is enhanced as both perturbations contribute to it.

Figure 11 indicates that a symmetric NSR spectrum similar to that shown in plot (i) is unlikely to be observed because of the influence of 3OD and IPRS. Indeed, the blue NSR peak was found to be more intense than the red one in a recent experiment[43]. The simple IPRS model based on eq. (16) is reasonably accurate when the picosecond pulse is concerned. A comprehensive study for the ultrashort pulse can only be possible with the use of eq. (3), which represents the generalized NLSE.

Figure 12 demonstrates how the relative values of 3OD and 4OD dispersion coefficients significantly affect the generation of DWs when the propagation dynamics of an ultrashort pulse is governed by eq. (3). The radiation peak and frequency positions both dramatically change with changing relative values of 3OD and 4OD coefficients. In our study we try to capture the evolution of amplitude as well as frequency positions of the radiation.

Figure 13 shows almost identical features that we have observed in the previous case (Figure 9), where the 3OD term is responsible for the generation of NSR. The only difference we get in this case is the dual radiation. In Figure 13 *a*, the solid curves represent the analytical predictions based on eq. (15), whereas open circles show simulated values obtained through the solution of eq. (3). The close agreement justifies the use of the phase-matching

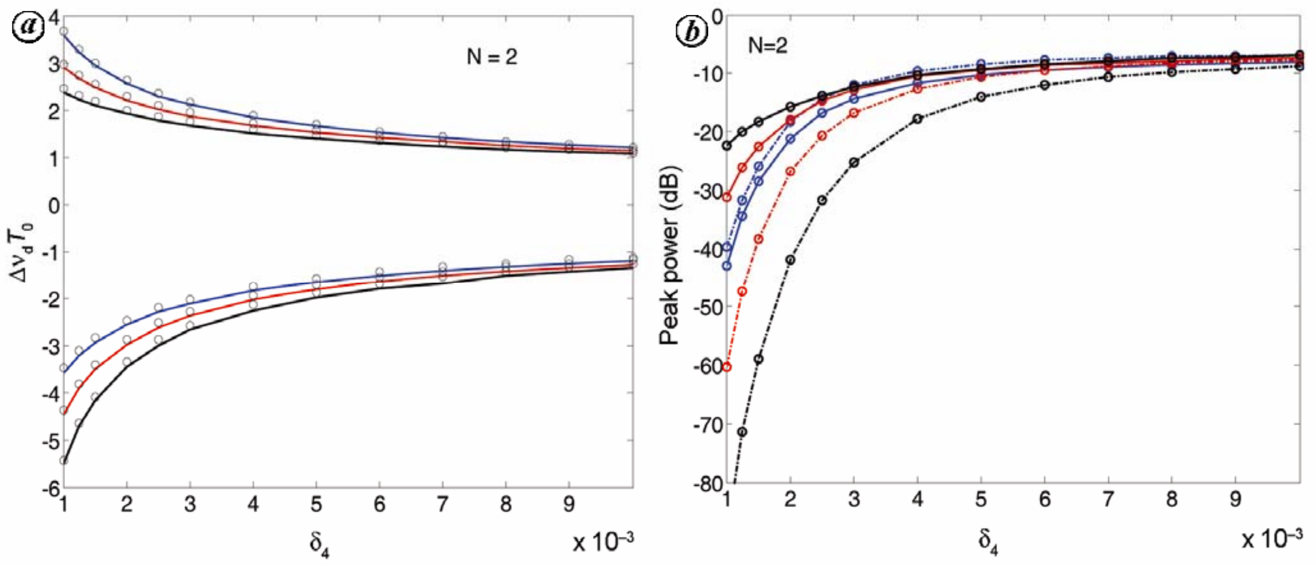

Figure 13. Frequency (***a***) and relative peak powers (***b***) of the red and blue NSR peaks plotted as a function of δ_4 for three values of δ_3. The blue, red and black lines are for $\delta_3 = 0$, $\delta_3 = 0.01$ and $\delta_3 = 0.02$ respectively. Open circles show the numerical values and solid lines represent the analytical prediction. ***b***, Solid lines and the dot-dashed lines represent the peak powers of the red and blue NSR peaks respectively.

matching condition given in eq. (15) and indicates that the IPRS process does not affect the NSR frequencies. Figure 13 suggests that for a fixed 3OD coefficient, with increasing δ_4 both the frequencies (red and blue) of the NSR become closer to the input frequency and their relative spacing eventually becomes constant. On the other hand, peak amplitude of the radiation increases to reach a saturation point with increasing 4OD coefficient. We further examine the growth of DW for a third-order soliton ($N = 3$) and find identical growth that we already have for $N = 2$ (ref. 44). The phase-matching condition as proposed in eq. (15) also holds good for $N = 3$.

At this point, it should be mentioned that the appearance of two zero-dispersion wavelengths (ZDW) in the fibres is connected with the dominance of the 4OD term that leads to the conjugate radiations on both sides of the input spectrum. Properly designed PCFs may possess this special dispersion characteristic. Soliton spectral tunnelling (SST) is another interesting phenomenon[45,46] that occurs with this kind of dispersion behaviour when two anomalous dispersion regions are separated by an intermediate normal dispersion zone. In Figure 14, the formation of SST is shown for a typical dispersion profile. Physically, a soliton formed in one anomalous dispersion region transfers its energy to a linear wave at a resonance frequency near the other zero-dispersion point. This sharp switching of soliton frequency from one anomalous dispersion domain to the other is interpreted by analogy with quantum mechanical tunnelling through a potential barrier[47]. Apart from the SST effect, SC generation in a PCF with two ZDWs has been studied extensively[48–50], where issues related to dual pumping[48], soliton-pair generation[49], etc. are considered, but not explicitly the issues related to DW generation which we try to explain more elaborately.

Role of HOD in generation of DW

So far we have studied the influence of 3OD and 4OD on the evolution of DWs. In this section, we look at the influence of individual and collective HOD terms in generating DWs based on normalized phase-matching condition as already mentioned in eq. (15). It is demonstrated that all positive even-order dispersion terms (i.e. 4OD, 6OD, 8OD, etc.) emit conjugate radiations. No such radiation is observed when the numeric sign of the even-order dispersion coefficients are set as negative. It can also be shown that all positive odd-order dispersion terms (i.e. 3OD, 5OD, 7OD, etc.) are capable of generating blue radiation. The radiation falls on the red side when the sign of the odd dispersion coefficient is reversed. A detailed analysis based on a numerical solution of the generalized NLSE confirms these features associated with DWs (ref. 51). The range of dispersion values that are used in our study are obtained from the design of realistic PCFs, indicating tremendous flexibility in dispersion tailoring.

The numerical solutions of the generalized NLSE as given in eq. (3) exhibit exciting results when different HOD terms are included in the simulation. The study shows dramatic modifications of NSRs with changing individual values of different HOD terms. In Figure 15 *a* we represent the output spectrum of a launched second-order soliton ($N = 2$) at a normalized distance $\xi = 2$ for $\delta_3 = 0.01$ and $\delta_4 = 0.0015$ with the other HOD terms set to zero. Two distinct DW peaks on the blue and red sides

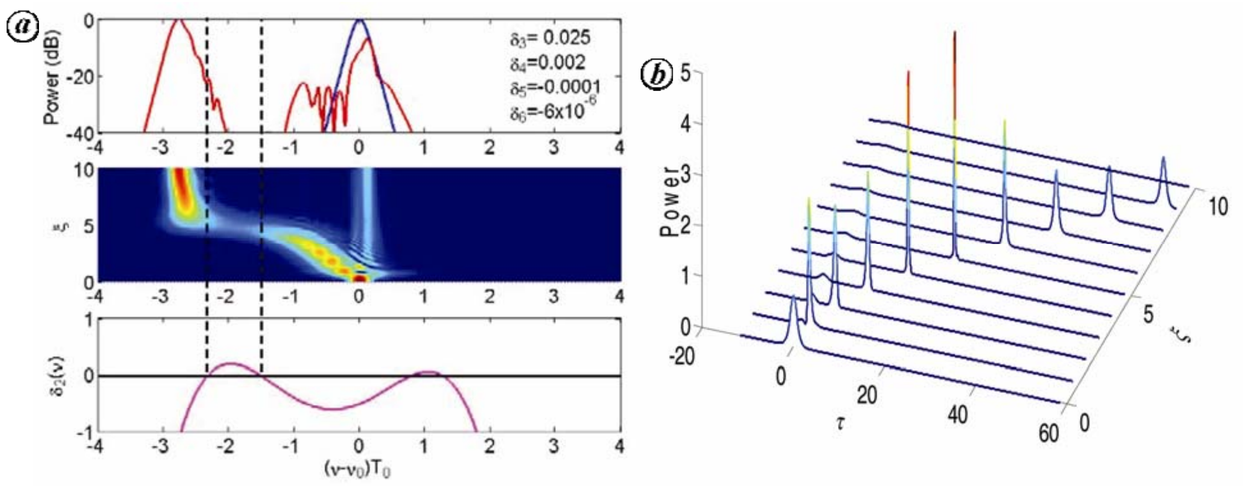

Figure 14. ***a***, A typical example of soliton spectral tunnelling for an arbitrary dispersion profile with soliton order $N = 2$. ***b***, The corresponding temporal evolution shows that the optical soliton becomes narrower and stronger at the point of tunnelling (roughly around $\xi = 5$).

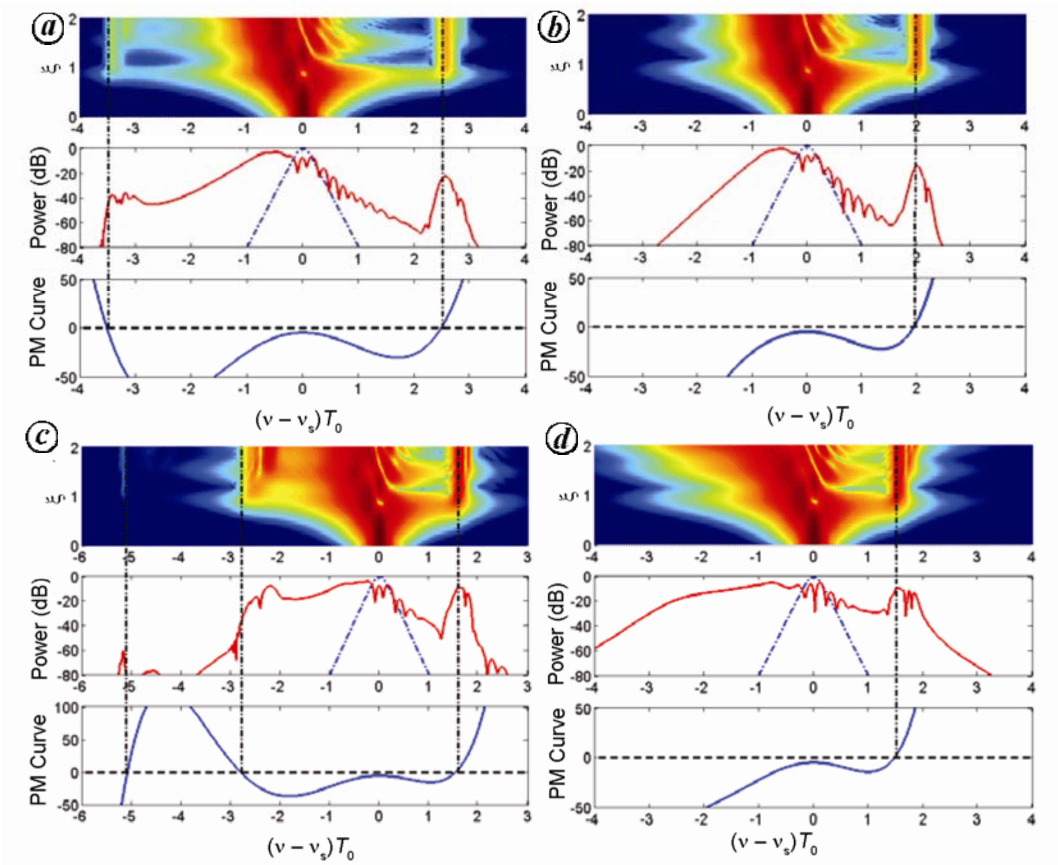

Figure 15. The contour and output spectra of a second-order soliton ($N = 2$) at two dispersions lengths. The phase-matching curve is plotted simultaneously. The dimensionless dispersion coefficients used in the plots are: (***a***) $\delta_3 = 0.01$, $\delta_4 = 0.015/10$, $\delta_5 = 0$, $\delta_6 = 0$; (***b***) $\delta_3 = 0.01$, $\delta_4 = 0.015/10$, $\delta_5 = 0.01/100$, $\delta_6 = 0$; (***c***) $\delta_3 = 0.01$, $\delta_4 = 0.04/10$, $\delta_5 = 0.01/100$, $\delta_6 = 0$, and (***d***) $\delta_3 = 0.01$, $\delta_4 = 0.04/10$, $\delta_5 = 0.015/100$, $\delta_6 = 0$.

are observed under such conditions. The phase-matching condition predicts the exact frequencies as shown in the bottom plot for the same set of parameters. The dual peaks arise due to the presence of 4OD.

In Figure 15 *b* it can be observed that with the incorporation of 5OD term, the red peak vanishes and interestingly, it reappears with an extra red peak (Figure 15 *c*) when the 4OD term is increased. Figure 15 *d*, again

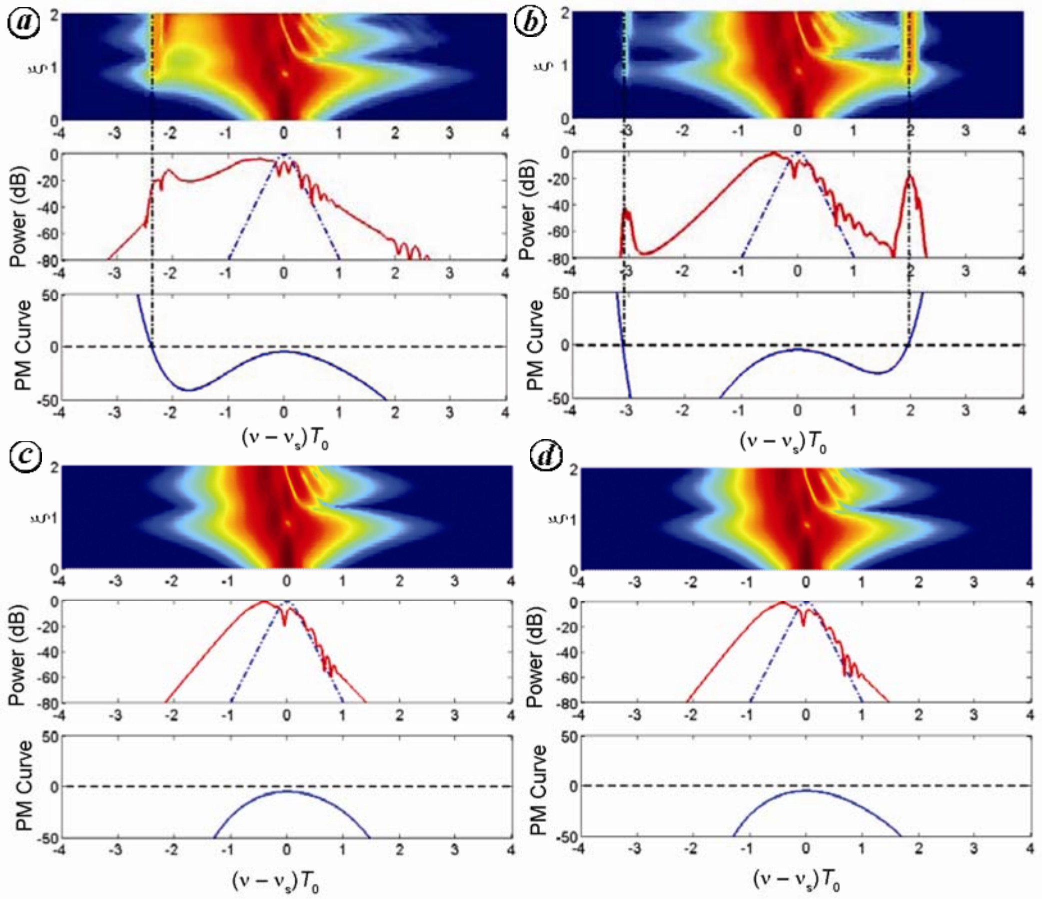

Figure 16. The contour and output spectra of a second-order soliton ($N = 2$) at two dispersion lengths. The phase-matching curve is plotted simultaneously. The dimensionless dispersion coefficients used in the plots are: (***a***) $\delta_3 = 0.01$, $\delta_4 = 0.015/10$, $\delta_5 = -0.01/100$, $\delta_6 = 0$; (***b***) $\delta_3 = 0.01$, $\delta_4 = 0$, $\delta_5 = 0.01/100$, $\delta_6 = 0.01/1000$; (***c***) $\delta_3 = 0.01$, $\delta_4 = -0.015/10$, $\delta_5 = 0$, $\delta_6 = 0$, and (***d***) $\delta_3 = 0.01$, $\delta_4 = 0$, $\delta_5 = 0.01/100$, $\delta_6 = -0.01/1000$.

shows how the red peaks vanish on further increment of the 5OD coefficient. More importantly, in all the cases the frequency of the radiation changes significantly and can be predicted quite accurately by the proposed normalized phase-matching expression given by the blue curve. The overall results given in Figure 15 unfold certain important facts; for example, the positive odd-order dispersion terms always try to generate blue radiation, whereas positive even-order dispersion terms exhibit dual radiation.

The negative HOD coefficient significantly affects the radiation frequencies. Figure 16 *a* shows how the radiation falls in the red side by inversing the sign of the 5OD term. In fact, we have verified this effect for other odd-order dispersion terms by inverting their numeric signs. Another striking feature which we observe is that negative even HOD terms never create any dual conjugate resonant DW. For negative even HOD terms there are no real roots of phase-matching equation. Hence under such a situation it is not possible to generate any DW. In Figure 16 *c* and *d*, we show this effect for negative 4OD and 6OD respectively. The physical parameters are the same as those used in Figures 15 *a* and *b* and 16 *a* and *b* except the negative sign of the 4OD and 6OD coefficients. The spectrum generated through the direct simulation of NLSE also predicts no peak generation under such condition.

Role of dispersion profile in controlling DWs

In the preceding section we concluded that every positive, even-order dispersion generates dual radiation, whereas every odd-order dispersion generates single radiation in the form of DW, and radiation frequency falls on the red or blue side of the operating frequency based on the negative and positive sign of the odd-order dispersion coefficients respectively. No radiation is expected to be generated for negative, even-order dispersion coefficients. Interpretation of the overall dispersion property was not considered in the study. We mainly concentrated on the individual value of dispersion coefficients, but the overall dispersion profile involving those individual dispersion coefficients was not taken into account.

In this section we show how the dispersion profile practically controls the generation of DWs. Now along

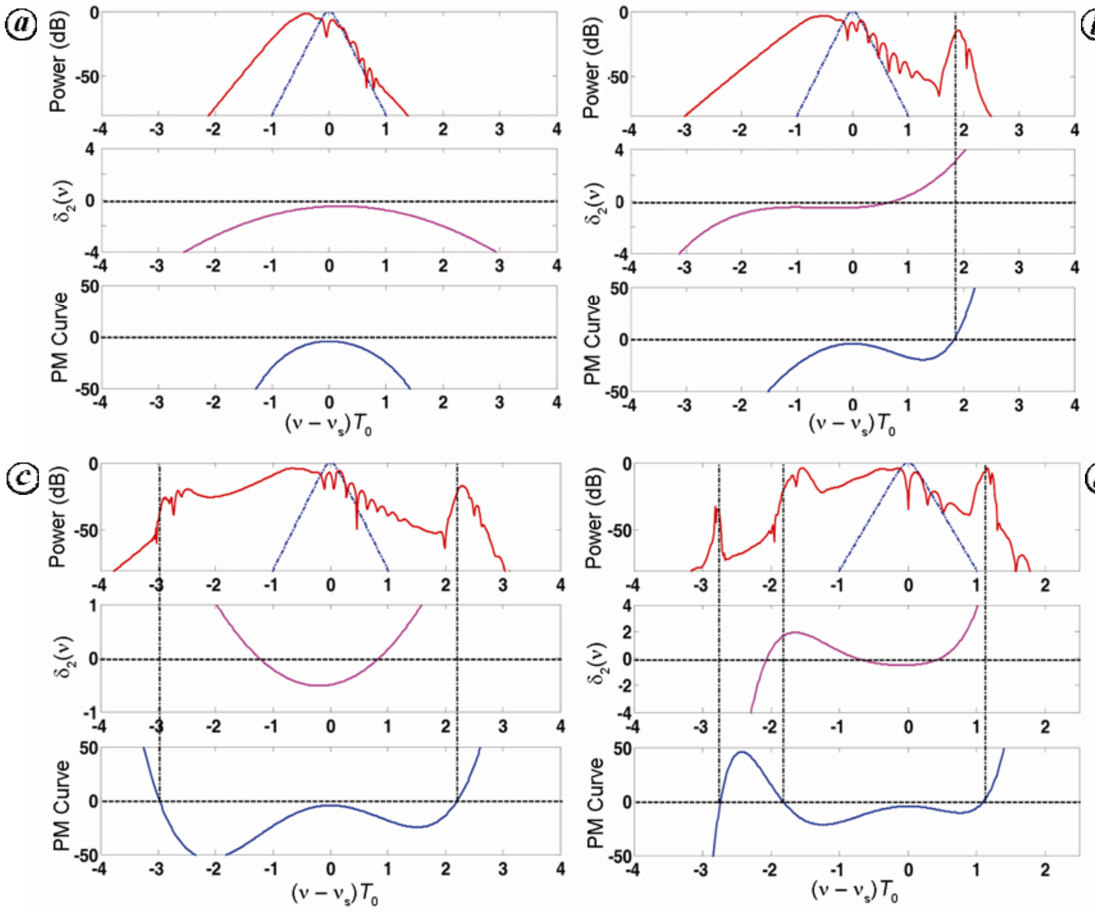

Figure 17. DW generation for different group velocity dispersion (GVD) profiles. ***a***, No NSR occurs as GVD curve does not have any zero dispersion point (ZDP). ***b***, Single radiation as GVD curve cuts the zero line once. ***c***, Dual radiation as GVD curve has two ZDPs. ***d***, Three radiations correspond to three ZDPs in the dispersion profile.

with the phase-matching curve we simultaneously plot the overall normalized dispersion ($\delta_2(\nu)$) profile to get an idea about the chosen dispersion coefficients. In fact expanding GVD as a Taylor series, one can readily predict the overall dispersion profile for the given dispersion coefficients at operating wavelength. In normalized form the 2OD can be expressed through the Taylor series as follows

$$\delta_2(x) = \frac{1}{2}\mathrm{sgn}(\beta_2) + \frac{1}{2}\sum_{m=1}^{\infty}\frac{(m+2)!}{m!}\delta_{m+2}x^m, \tag{17}$$

where $x = 2\pi(\nu - \nu_s)T_0$, which has been already defined. The study reveals that the number of DWs generated in a spectrum is equal to the number of zero crossing points of $\delta_2(x)$ that is, the number of zero dispersion wavelengths present in the fibre. For example, if we get a dual radiation then the corresponding fibre must have two zero dispersion wavelengths. Figure 17 clearly indicates how zero dispersion points (ZDPs) present in a specific dispersion profile become an excellent predictors of the number of DW peaks present in the output spectra. We examine numerically dispersion profiles with as many as six ZDPs and find that this criterion always holds.

Another interesting feature we find is the generation of dual radiation on a single side. So far in all cases we observed that for dual radiation one can simultaneously have one blue and one red peak. But it is possible to generate two blue or two red peaks simultaneously by special dispersion profile. The observation suggests that for a fibre if both the ZDPs fall on the higher frequency side compared to the operating frequency, then one may expect two blue radiations. That means both the radiations fall in the higher frequency side compared to ν_s, the operating frequency. This behaviour is shown in Figure 18 *a*. Conversely, if both the 2DPs fall on the lower frequency side of the soliton frequency ν_s, then one would expect two red peaks. Figure 18 *b* shows this condition. With this result it may be concluded that, if the zero dispersion frequency is greater than operating frequency, then always blue radiation will be generated, whereas one may expect red radiation if the zero dispersion frequency is less than the input soliton frequency.

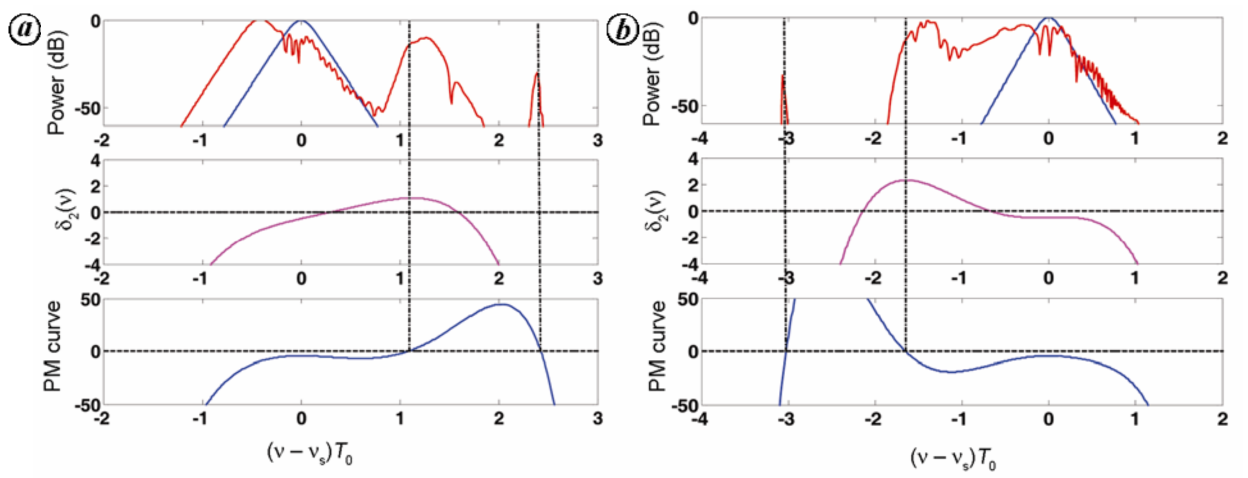

Figure 18. Dual radiation at the blue side (***a***) and red side (***b***). In both cases, the operating frequency falls in the anomalous dispersion domain.

DW generation under normal GVD pumping

In all the preceding cases, we have considered the operating wavelength in anomalous dispersion domain in order to study the NSR. We assume this condition because the soliton can form only in anomalous dispersion domain, whereas in a previous study[7] it has been established that soliton fission has an important role in the generation of DW. Hence it is fairly justified to consider input pulse in anomalous dispersion domain for the study of DW because the optical soliton can only be constructed in such a condition. However, at this point the question must be asked whether there is any possibility to generate DW under normal GVD pumping. Interestingly, our numerical study reveals that DW maybe generated even under normal GVD pumping at relatively longer distance. However, we notice that the phase-matching condition does not accurately determine the frequency of the radiation peak because of the extinction of soliton fission phenomenon under normal GVD pumping.

It has been already mentioned that SST is an important mechanism that can generate a DW-type radiation when a soliton tunnels from one anomalous dispersion region to another, separated by an intermediate region of normal dispersion[45–47]. A localized inhomogeneity of the GVD is responsible for SST to occur. In our case, the situation was different because we had launched a pulse in the normal dispersion regime. However, the pulse experiences considerable spectral broadening, primarily through self-phase modulation, which broadens the pulse spectrum symmetrically on both sides of the input spectrum. At some point, a part of the pulse energy enters the anomalous dispersion region where a soliton can form. The question one may ask is whether the formation of this soliton is accompanied with the emission of some radiation. Our numerical results indicate that this is the case. In Figure 19 *a* we plot the output spectrum of a femtosecond pulse launched in the normal dispersion regime of a fibre with $\delta_3 = 0.05$, $\delta_4 = -0.01$ and $\delta_5 = 0.0005$ (all other higher-order coefficients set to zero). The spectrum indicates a distinct peak around 1.65 (in normalized unit) that is generated roughly at the same distance into the fibre where a soliton forms with the spectrum on the red side. This behaviour is clearly seen in the middle part of Figure 19 *a*. The abrupt change in the sign of the dispersion slope (δ_3 shown by the green curve) disturbs the monotonous broadening of the spectrum and creates a distinct spectral peak on the blue side. This behaviour is similar to the soliton tunnelling effect, but we cannot call it soliton tunnelling because most of the pulse energy lies in the normal dispersion region. It should be noted that the phase-matching condition (shown by a blue curve) does not accurately predict the frequency of this radiation.

After DW has been generated, a part of the pulse spectrum lies in the anomalous region and can form a soliton. The temporal evolution in Figure 19 *b* shows the soliton formation clearly, where a part of the pulse energy is delayed by a large amount (as much as by 120 T_0). This delay can be understood by noting that the soliton spectrum is shifted towards the red side and that longer wavelengths travel slower in the anomalous dispersion region.

We have found a second mechanism of DW generation. An extensive numerical study covering a wide range of operating conditions, reveals that DWs can still be generated for a few specific dispersion profiles chosen, such that a narrow normal dispersion region is surrounded on both sides by anomalous regions. In this case, SPM-induced spectral broadening forces most of the pulse energy to travel in the anomalous regions as a soliton after some distance along the fibre. After that, a DW can be generated through soliton fission. This situation is illustrated in Figure 19 *c* by changing the dispersion parameters ($\delta_3 = 0.01$, $\delta_4 = -0.01$ and $\delta_5 = 0.0005$) from those used in Figure 19 *a* such that the normal GVD region is

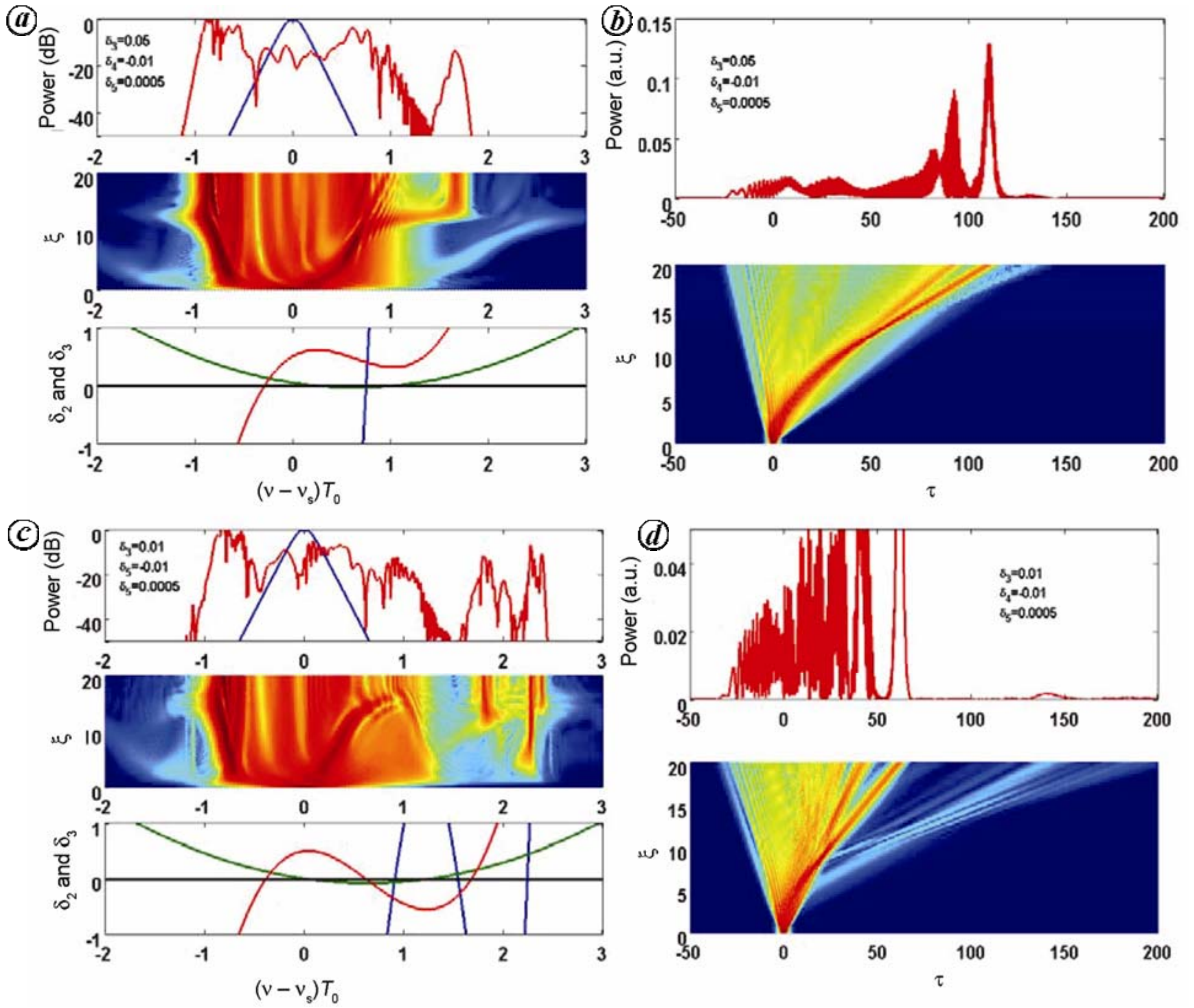

Figure 19. Spectral tunnelling effect when the input pulse is launched in the normal GVD region of the fibre with $N = 3$. ***a***, Output spectrum (top), spectral evolution (middle) and GVD profile (red), dispersion slope (green) and phase-matching expression (blue) of the fibre (bottom) shown for the parameters $\delta_3 = 0.05$, $\delta_4 = -0.01$ and $\delta_5 = 0.0005$. ***b***, Output pulse shapes and temporal evolution inside the fibre depicted when the fibre is pumped at normal GVD domain. ***c***, ***d***, Plots corresponding to different parameters ($\delta_3 = 0.01$, $\delta_4 = -0.01$ and $\delta_5 = 0.0005$) for which the DW peak forms on the blue side of the input spectrum. In both the cases third-order soliton is used as input.

surrounded on both sides by anomalous domains (red curve). We now find two distinct spectral peaks at frequencies 1.8 and 2.25 (in normalized units). The peak at 1.8 is due to the tunnelling phenomenon discussed earlier. The new peak at 2.25 is due to a DW emitted through soliton fission and satisfies the phase-matching condition in eq. (15). The time domain evolution in Figure 19 *d* shows clearly how a DW is emitted near $\xi = 10$ with a large blue shift. Because its frequency falls in the normal dispersion region where blue-shifted components travel slower than the red-shifted ones, this DW is delayed and appears at $\tau \approx 140$ at the output end of the fibre.

The blue-shifted DW peak vanishes when the dispersion parameters of the fibre are changed slightly to $\delta_3 = 0.01$, $\delta_4 = -0.01$ and $\delta_5 = 0.000325$. This case is shown in Figure 20 *a*. For this set of parameters, even though most of the pulse energy eventually enters the anomalous dispersion region, there is no solution of the phase-matching condition that can create a DW (see the blue curve). The time domain evolution shown in Figure 20 *b* also supports this argument by exhibiting no trace of a DW radiation. The peak due to the tunnelling effect is still observed, but its position is now shifted around 1.4 (in normalized units). In Figure 20 *c* we manipulate the dispersion curve (red line) in such a manner that it exhibits three ZDPs with a narrow anomalous dispersion zone falling in the lower frequency side surrounded by two normal dispersion zones. For this configuration, we calculate δ_3 (green line) as well as the phase-matching condition (blue line). The phase-matching condition exhibits a DW solution around the normalized frequency of –2.25. The spectral evolution indeed shows such a red-shifted DW peak. The time domain evolution also shows a DW peak of low amplitude around $\tau = -100$, i.e. DW travels

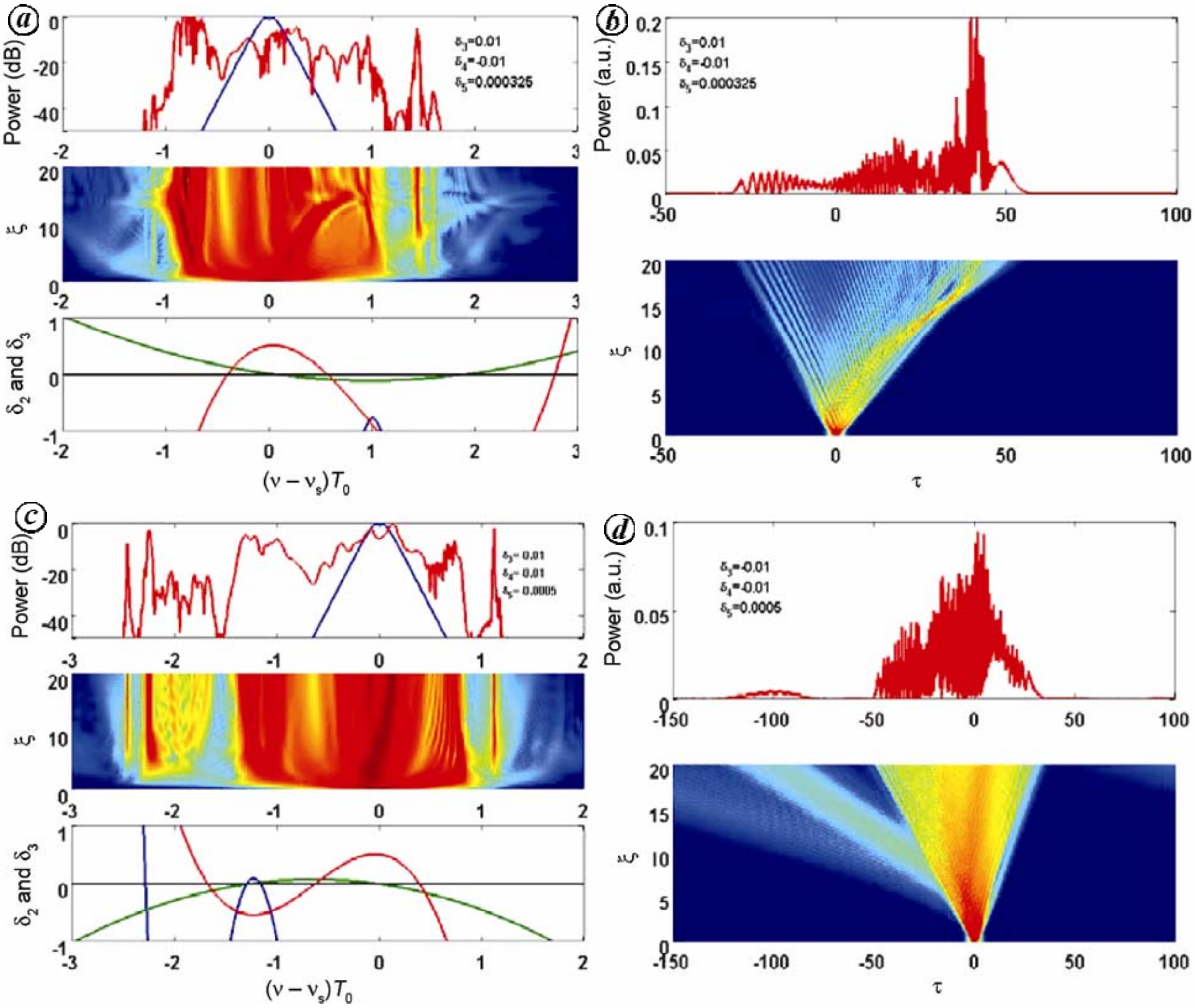

Figure 20. Different dispersion values used in order to understand the spectral evolution under normal GVD pumping with soliton order $N = 3$. ***a***, The parameters used are: $\delta_3 = 0.01$, $\delta_4 = -0.01$ and $\delta_5 = 0.000325$. No phase-matching solution can be obtained for these parameters and hence generation of DW ceases to exist. ***b***, Time domain evolution does not exhibit any radiation. ***c***, Formation of DW in red side shown for the following normalized dispersion coefficients: $\delta_3 = -0.01$, $\delta_4 = -0.01$ and $\delta_5 = -0.0005$. ***d***, Time domain evolution exhibits radiation as a pedestal around $\tau \approx -100$.

faster than other parts of the pulse. This is understood by noting that GVD is normal at the DW frequency where red components travel faster than the blue components. We must emphasize that the traditional phase-matching expression generally fails when the optical pulse propagates entirely in the normal GVD domain. However, if most of the pulse energy enters the anomalous GVD regime, it can be used to predict the formation of DWs. The tunnelling effect, on the other hand, takes place in a concurrent manner that exhibits additional fringes. It can be shown that no such radiation is possible if the GVD profile grows monotonically without any change in sign.

Experiment of DW generation

In the previous sections we have studied the generation of NSR theoretically based on the solution of generalized NLSE and the corresponding phase-matching condition. We chose arbitrarily the numerical values of HOD terms to produce the specific dispersion profile and investigated DW generation for that profile using the solution of the generalized NLSE. We even assign zero value of different HOD terms during the numerical calculation to visualize the role of individual dispersion terms on DW generation. However, in practice it is difficult to excite a definite dispersion order by suppressing other. A relatively complicated structure may be required to achieve the desired dispersion profile where certain HOD terms predominate. Generally, all HOD terms contribute in the extended Taylor series expansion, which typically describes the overall dispersion profile. Nevertheless, the profile can be tailored significantly for PCF waveguides. In Figure 21, we represent the experimental output spectra of SC for highly nonlinear PCFs fabricated at CGCRI. The effective refractive index over different wavelengths

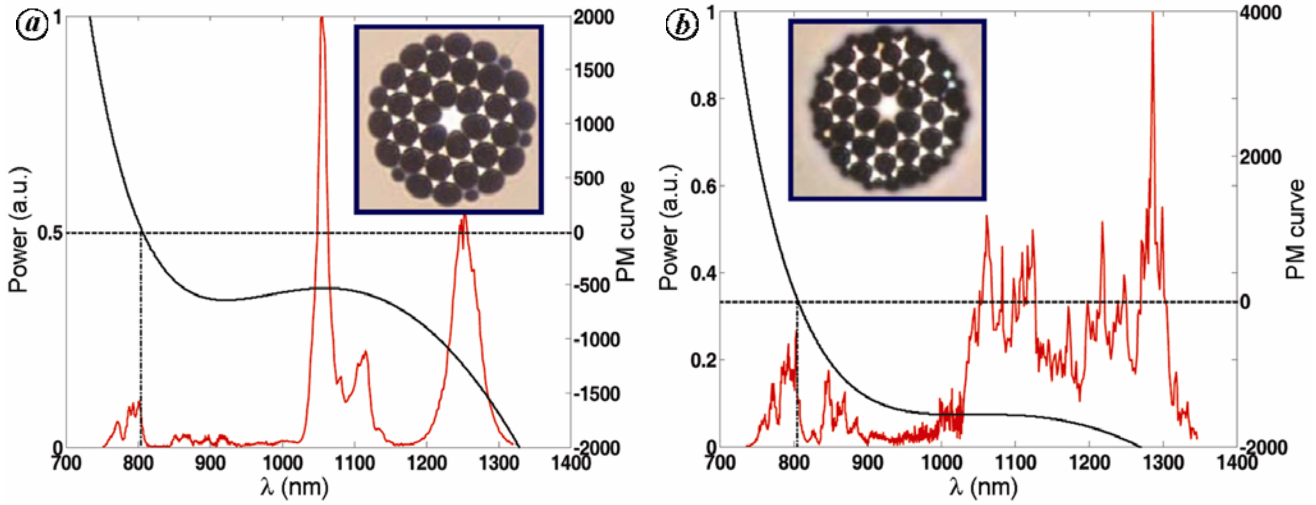

Figure 21. Experimental spectra showing DW around 800 nm. The phase-matching curve (black solid line) based on eq. (15) exactly predicts the DW in both cases. (Inset) Cross-sections of the PCF used. The input energies for (***a***) and (***b***) are 4.5 and 110 nJ respectively, and in both the cases 30 cm of PCF is used. For both cases pump wavelength falls in the anomalous dispersion domain.

and nonlinearity of the two designed PCFs were calculated using COMSOL Multiphysics, a commercial software based on FEM. Further, for both cases, we have calculated the corresponding phase-matching condition taking up to eighth order of dispersion coefficients and predicted the DW around 800 nm. As shown in Figure 21, the experimental spectra also produce the dispersive radiation around that wavelength. The zero dispersion wavelengths for the two PCFs have been calculated as 987 nm (Figure 21 *a*) and 1040 nm (Figure 21 *b*) respectively, and the pump wavelength used is 1060 nm. It should be noticed that for both the cases, the NSR falls on the same side that of the ZDP as theoretically predicted. In practice, DWs are frequently identified as a blue radiation because of the fact that for the general dispersion profile ZDP falls in the lower wavelength side with respect to operating wavelength, which is in the anomalous GVD regime. However, it is realistic to design the desired dispersion profile in PCFs to achieve specific DW peaks in the output spectra. The present theoretical study may be a useful guideline to enhance and control the SC bandwidth by modifying design parameters of PCF.

Conclusion

The SC generation is a complex process where some typical nonlinear phenomena are involved, which should be taken into account for further studies. Several interesting processes are involved in the generation of SC and the origin of DW is one of them. The extreme blue component of the wide SC band is mainly generated through DW or NSR. A detailed study reveals that HOD produces a perturbation in the stable propagation of higher order soliton. As a result, some energy is transferred from the soliton to narrow band resonance. The frequency of such a radiation is immediately predicted through the phase-matching condition when an ultrashort pulse is pumped under anomalous GVD regime. The specific role of different orders of dispersion in generating DWs was studied extensively and it was found that 3OD is the primary term in creating DWs. The growth and frequency of radiation critically depend on 3OD. It has been shown that with increasing 3OD parameter the peak intensity of the radiation gradually increases and finally saturates. On the other hand, 4OD is responsible for dual radiation symmetrically placed in the frequency domain. However, the presence of 3OD and higher-order nonlinear effects destroys this symmetry. The growth of the radiation peaks follows is identical to that observed in the case of 3OD. A more important inference is drawn when we include other HOD terms to generalize our study. We find that all odd, HOD terms (i.e. 3OD, 5OD, etc.) generate a single DW peak on the blue or the red side of the carrier frequency, depending on whether the odd-order dispersion coefficient has a positive or negative sign. On the other hand, the positive, even, HOD terms (i.e. 4OD, 6OD, etc.), create conjugate DW peaks, one on the blue and the other on the red side. Interestingly, for negative values of the even HOD coefficients, no real solution of the phase-matching equation is possible, and hence no DW radiation is emitted under such conditions. A further study reveals that there is a close correlation among the overall dispersion profiles and NSR. Detailed simulations indicate that the number of ZDPs present in a specific dispersion profile is an excellent predictor of the number of dispersive peaks to be created in the output pulse spectrum. A fibre with a single ZDP has only one DW peak, and a fibre with two ZDPs always exhibits dual DW peaks. Moreover, no DW can be expected in a fibre that has no zero-dispersion crossings over the entire range of wavelengths. We have examined numerically dispersion profiles with as many as six ZDPs and have found that this criterion always holds. Another interesting feature we noticed is that, if the frequency of ZDP is larger (smaller) than the operating frequency, DWs fall on the higher (lower) frequency side of the operating frequency. Therefore, there is a possibility of generating two DW peaks on the same side (blue or red side) of the output pulse spectrum by tailoring the dispersion curve suitably. Finally, it is demonstrated that DWs can be generated under normal GVD pumping. Based on the results and discussion presented in this article we are now in a position to provide guidelines that would improve the experimental designs which are specifically targeted to enhance DW radiations at extreme edges of the SC spectra.

1. Dudley, J. M., Genty, G. and Coen, S., Supercontinuum generation in photonics crystal fiber. *Rev. Mod. Phys*., 2006, **78**, 1135–1184.
2. Zheltikov, A. M., Let there be white light: supercontinuum generation by ultrashort laser pulses. *Phys–Uspekhi*, 2006, **49**, 605–628.
3. Dudley, J. M. and Taylor, J. R., Ten years of nonlinear optics in photonic crystal fiber. *Nature Photonics*, 2009, **3**, 85–90.
4. Agrawal, G. P., *Nonlinear Fiber Optics*, Academic Press, California USA, 2008, 4th edn.
5. Hasegawa, A. and Matsumoto, M., *Optical Solitons in Fibers*, Springer, Berlin, 2002, 3rd edn.
6. Wai, P., Menyuk, C., Lee, Y. and Chen, H., Nonlinear pulse propagation in the neighborhood of the zero dispersion wavelength of monomode optical fibers. *Opt. Lett*., 1986, **11**, 464–466.
7. Akhmediev, N. and Karlsson, M., Cherenkov radiation emitted by solitons in optical fibers. *Phys. Rev. A*, 1995, **51**, 2602–2607.
8. Knight, J. K., Birks, T., Russell, P. St. J. and Atkin, D. M., All-silica single-mode optical fiber with photonic crystal cladding. *Opt. Lett*., 1996, **21**, 1547–1549.
9. Knight, J. K., Photonic crystal fibers. *Nature*, 2003, **424**, 847–851.
10. Russell, P. St. J., Photonics crystal fibers. *Science*, 2003, **299**, 358–362.
11. Russell, P. St. J., Photonics-crystal fibers. *IEEE J. Lightwave Tech*., 2006, **24**, 4729–4749.
12. Saitoh, K. and Koshiba, M., Numerical modeling of photonic crystal fiber. *IEEE J. Lightwave Tech*., 2005, **23**, 3580–3591.
13. Poletti, F. and Horak, P., Dynamics of femtosecond supercontinuum generation in multimode fibers. *Opt. Exp.*, 2009, **17**, 6134–6147.
14. Nishizawa, N. and Goto, T., Pulse trapping by ultrashort soliton pulses in optical fibers across zero-dispersion wavelength. *Opt. Lett*., 2002, **27**, 151–154.
15. Knight, J. C., Birks, T. A. and Russell, P. St. J., Holey silica fibers. In *Optics of Nanostructured Materials* (eds Markel, A. V. and George, T.), Wiley, 2001.
16. Frampton, K. E. *et al.*, Fabrication of microstructured optical fiber. World Intellectual Property Organization (PCT), WO 03/078339 A1, 25 September 2003.
17. Borelli, N. F., Wright Jr, J. F. and Wusirika, R. R., Method of fabricating photonic structures. U.S. Patent 6 496 632, 17 December 2002.
18. Jackobsen, C., Vienne, G. and Hansen, T. P., Preform method of its production, and use thereof in production of microstructured optical fibers. World Intellectual Property Organization (PCT), WO 03/078338 A2, 25 September 2003.
19. Hasegawa, T., Onishi, M., Sasaoka, E. and Nishimura, M., Optical fiber and method for making the same. U.S. Patent 6 766 088, 20 July 2004.
20. Benabid, A. F. and Knight, J. C., Improvements in and relating to microstructured optical fibers. World Intellectual Property Organization (PCT), WO 2004/001461 A1, 31 December 2003.
21. Broeng, J., Barkou, S. E. and Bjarklev, A. O., Microstructured optical fibers. World Intellectual Property Organization (PCT), WO 99/064903, 16 December 1999.
22. Russell, P. J., Birks, T. A., Knight, J. C. and Mangan, B. J., Photonic crystal fiber and a method for its production. World Intellectual Property Organization (PCT), WO 00/060388, 12 October 2000.
23. Fitt, A. D., Furusawa, K., Monro, T. M. and Please, C. P., Modeling the fabrication of hollow fibers: capillary drawing. *J. Lightwave Technol*., 2001, **19**, 1924–1931.
24. Xue, S. C., Large, M. C. J., Barton, G. W., Tanner, R. I., Poladian, L. and Lwin, R., Role of material properties and drawing conditions in the fabrication of microstructured optical fibers. *J. Lightwave Technol.*, 2006, **24**, 853–860.
25. Husakou, A. V. and Herrmann, J., Supercontinuum generation of higher order solitons by fission in photonic crystal fibers. *Phys. Rev. Lett*., 2001, **87**, 203901.
26. Herrmann, J. *et al.*, Experimental evidence for supercontinuum generation by fission of higher order soliton in photonic fibers. *Phys. Rev. Lett*., 2002, **88**, 173901.
27. Lin, Q. and Agrawal, G. P., Raman response function for silica fibers. *Opt. Lett*., 2006, **31**, 3086–3088.
28. Elgin, J. N., Soliton propagation in an optical fiber with third order dispersion. *Opt. Lett*., 1992, **17**, 1409–1411.
29. Höök, A. and Karlsson, M., Ultashort solitons at minimum-dispersion wavelength: effect of fourth order dispersion. *Opt. Lett.*, 1993, **18**, 1388–1390.
30. Elgin, J. N., Perturbations of optical solitons. *Phys. Rev. A*, 1993, **47**, 4331–4341.
31. Karpman, V. I., Radiation of soliton by higher order dispersions. *Phys. Rev. E*, 1993, **47**, 2073–2082.
32. Husakou, A. and Herrmann, J., Supercontinuum generation, four wave mixing and fission of higher order soliton in photonic crystal fibers. *J. Opt. Soc. Am. B*, 2002, **19**, 2171–2182.
33. Blanch, A. O., Knight, J. C. and Russell, P. St. J., Pulse breaking and supercontinuum generation with 200 fs pump pulses in photonic crystal fibers. *J. Opt. Soc. Am. B*, 2002, **19**, 2567–2572.
34. Dudley, J. M. *et al.*, Cross-correlation frequency resolved optical grating analysis of broadband continuum generation in photonic crystal fiber: simulation and experiments. *Opt. Express*, 2002, **10**, 1215–1221.
35. Tartara, L., Cristiani, I. and Degiorgio, V., Blue light and infrared continuum generation by soliton fission in a microstructured fiber. *Appl. Phys. B*, 2003, **77**, 309–311.
36. Hilligsøe, K. M., Paulsen, H. N., Thrøgersen, J., Keidsen, S. R. and Larsen, J. J., Initial steps of supercontinuum generation in photonic crystal fibers. *J. Opt. Soc. Am. B*, 2003, **20**, 1887–1893.
37. Cristiani, I., Tediosi, R., Tartara, L. and Degiorgio, V., Dispersive wave generation by solitons in microstructured optical fibers. *Opt. Express*, 2003, **12**, 124–135.
38. Genty, G., Lehtonen, M. and Ludvigsen, H., Effect of cross-phase modulation on supercontinuum generated in microstructured fibers with sub-30 fs pulses. *Opt. Express*, 2004, **12**, 4614–4624.
39. Eflimov, A. *et al.*, Interaction of an optical soliton with dispersive waves. *Phys. Rev. Lett*., 2005, **95**, 213902.
40. Skryabin, D., Luan, F., Knight, J. K. and Russell, P. St. J., Soliton self frequency shift cancellation in photonic crystal fibers. *Science*, 2003, **301**, 1705–1708.
41. Biancalana, F., Skryabin, D. and Yulin, A., Theory of self frequency shift compensation by resonant radiation in photonic crystal fibers. *Phys. Rev. E*, 2004, **70**, 016615.

42. Roy, S., Bhadra, S. K. and Agrawal, G. P., Dispersive wave emitted by solitons perturbed by third order dispersion inside optical fiber. *Phys. Rev. A*, 2009, **79**, 023824.
43. Benaleid, F. *et al.*, Fourth-order dispersion mediated solitonic radiations in HC-PCF cladding. *Opt. Lett*., 2008, **33**, 2680–2683.
44. Roy, S., Bhadra, S. K. and Agrawal, G. P., Perturbation of higher order soliton by fourth order dispersion in optical fibers. *Opt. Commun*., 2009, **282**, 3798–3803.
45. Tsoy, E. N. and de Sterke, C. M., Theoretical analysis of self frequency shift near zero dispersion point: soliton spectral tunneling. *Phys. Rev. A*, 2007, **76**, 043804.
46. Poletti, F., Horak, P. and Richardson, D. J., Soliton spectral tunneling in dispersion controlled holy fiber. *IEEE Photonics Technol. Lett*., 2008, **20**, 1414–1416.
47. Kibler, B., Lacourt, P. A., Courvoisier, F. and Dudley, J. M., Soliton spectral tunneling in photonic crystal fiber with subwavelength defect. *IEEE Electron. Lett*., 2007, **43**, 967–968.
48. Schreiber, T., Andersen, T. V., Schimpf, D., Limpert, J. and Tunnermann, A., Supercontinuum generation by femtosecond single and dual wavelength pumping in photonic crystal fibers with two zero dispersion wavelengths. *Opt. Express*, 2005, **13**, 9556–9569.
49. Frosz, M. H., Falk, P. and Bang, O., The role of second zero dispersion wavelength in generation of supercontinuua and bright-bright soliton pairs across the zero dispersion wavelength. *Opt. Express*, 2005, **13**, 6181–6192.
50. Mussot, A., Beaugeois, M., Bouazaoui, M. and Sylvestre, T., Tailoring CW supercontinuum generation in microstructured fibers with two zero dispersion wavelengths. *Opt. Express*, 2007, **15**, 11553–11556.
51. Roy, S., Bhadra, S. K. and Agrawal, G. P., Effect of higher order dispersion on resonant dispersive waves emitted by solitons. *Opt. Lett.*, 2009, **34**, 2072–2074.

ACKNOWLEDGEMENTS. We thank Prof. Indranil Manna, Director, CGCRI, Kolkata for his permission to publish this paper. We also thank Debashri Ghosh, CGCRI and Prof. A. Kar and his group at Heriot-Watt University, Edinburgh, UK, for providing experimental details, and Dr M. Sreemany for taking the SEM micrograph of PCF. S.R. thanks Council of Scientific and Industrial Research, New Delhi for financial support to carry out this work.

Received 5 January 2010; revised accepted 15 December 2010